NPS 63-83-001

NAVAL POSTGRADUATE SCHOOL
Monterey, California

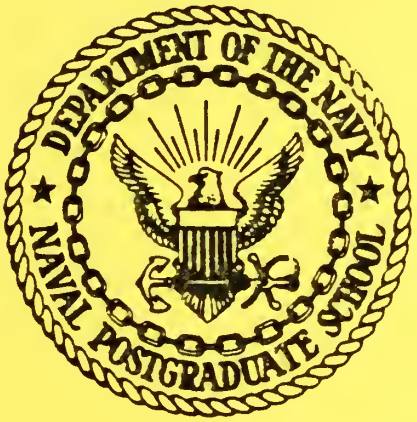

FURTHER STUDIES IN THE APPLICATION OF
DYNAMIC INITIALIZATION FOR GLOBAL
PREDICTION MODELS WITH SPECIAL ATTENTION
TO EQUATORIAL WAVES

by

F. J. Winninghoff and R. T. Williams

April 1983

Prepared for: Naval Environmental Prediction Research Facility
Monterey, California 93940

Naval Postgraduate School
Monterey, California 93940

Rear Admiral J. J. Ekelund
Superintendent

D. A. Schrady
Provost

The work reported herein was partially supported by the Naval Environmental Prediction Research Facility.

This report was prepared by:

Unclassified

SECURITY CLASSIFICATION OF THIS PAGE (When Data Entered)

REPORT DOCUMENTATION PAGE

READ INSTRUCTIONS BEFORE COMPLETING FORM

1. REPORT NUMBER: NPS63-83-001	2. GOVT ACCESSION NO.
3. RECIPIENT'S CATALOG NUMBER	
4. TITLE (and Subtitle): Further Studies in the Application of Dynamic Initialization for Global Prediction Models with Special Attention to Equatorial Waves	5. TYPE OF REPORT & PERIOD COVERED
	6. PERFORMING ORG. REPORT NUMBER
7. AUTHOR(s): F. J. Winninghoff and R. T. Williams	8. CONTRACT OR GRANT NUMBER(s)
9. PERFORMING ORGANIZATION NAME AND ADDRESS: Naval Postgraduate School Monterey, California 93940	10. PROGRAM ELEMENT, PROJECT, TASK AREA & WORK UNIT NUMBERS
11. CONTROLLING OFFICE NAME AND ADDRESS: Naval Environmental Prediction Research Facility Monterey, California 93940	12. REPORT DATE: March 1983
	13. NUMBER OF PAGES: 43
14. MONITORING AGENCY NAME & ADDRESS (if different from Controlling Office)	15. SECURITY CLASS. (of this report): Unclassified
	15a. DECLASSIFICATION/DOWNGRADING SCHEDULE

16. DISTRIBUTION STATEMENT (of this Report)

Approved for public release; distribution unlimited.

17. DISTRIBUTION STATEMENT (of the abstract entered in Block 20, if different from Report)

18. SUPPLEMENTARY NOTES

19. KEY WORDS (Continue on reverse side if necessary and identify by block number)

Initialization
Tropical waves
Numerical Weather Prediction

20. ABSTRACT (Continue on reverse side if necessary and identify by block number)

A dynamical initialization procedure incorporating friction and simulated heating has been applied with the use of a global barotropic primitive equation model in spherical coordinates to the problem of initialization of small scale motions in the fluid. Special emphasis is given to Kelvin and Rossby-gravity waves centered on the equator. These types of waves cause considerable difficulty if any type of quasi-geostrophic or "balanced" type of initialization is used. The results

DD FORM 1 JAN 73 1473 EDITION OF 1 NOV 65 IS OBSOLETE S/N 0102-014-6601

Unclassified

SECURITY CLASSIFICATION OF THIS PAGE (When Data Entered)

are very encouraging in the sense that if information concerning the wind fields associated with such waves is available the mass field can be recaptured quite well even if no information beyond its mean value is available.

For operational purposes some combination of this method with present advanced balancing methods may be indicated.

1. Introduction

With the ongoing development of larger and faster computers, global prediction using primitive equation models incorporating complex physics has, since 1975, become feasible (i.e. the European Mid Range Model, NMC's spectral model, the U.S. Navy NOGAPS model).

Based on work by Rossby dating as far back as 1938 and the subsequent work of Cahn (1945) concerning geostrophic adjustment, it was realized already in the early 1950's (Hinkleman, 1951), that initializing a primitive equation model with some form of a quasi-geostrophic balanced wind (in Hinkleman's early work - just the geostrophic wind itself) would be adequate to obtain useful forecasts since the geostrophic adjustment mechanism permitted by the primitive system would be able to keep the inertial-gravity wave amplitudes small relative to the Rossby wave amplitudes.

Due to increased understanding of how to properly control the development of nonlinear instability, practical primitive equation models were developed in the 1960's first for general circulation study (for which there was really no initialization problem) and then for operational forecasting. Increasingly refined methods for obtaining a balanced initial state have been developed. Recent among them have been the variational methods and the normal mode method. In the latter, the inertial-gravity waves and the mass and wind tendencies associated with them are explicitly removed from the initial fields (Machenhauer, 1977).

In the late 1960's another and quite simple initialization method, now known as dynamic initialization was proposed. Reference for it can be found in Nitta and Hovermale (1969), Miyakoda and Moyer (1968) or Winninghoff (1968, 1973a, 1973b). It enjoyed some attention, but because of its need for a large

amount of computer time, interest in it faded especially in comparison with the more efficient normal mode technique.

The purpose of the work which is reported on in the present paper was originally to extend the work in 1973b. Motivation also comes from the more advanced state of computer technology at present.

In 1973b, the author used a free surface global model with a $\underline{10^{\circ}\ \text{mesh}}$ size to investigate a dynamical initialization procedure. Results clearly indicated that restoration to the mass field in high latitudes, to the wind field in low latitudes and a blend of the two between 30° and 60° was very satisfactory for the purpose of reducing the amplitudes of the so called "noise" waves. Then an investigation was made concerning incorporation of heating and friction into the procedure. Here rather idealized circular symmetric tropical perturbations were used. The result clearly indicated the feasibility of doing this when the equations were run forward. The author was using a forward-backward iterative procedure. During the backward part, however, whether restoration be done to the total wind or just the nondivergent part was not clearly determined. The model's mesh size was too crude since the computer used at that time was very small compared to those available today.

The use of global prediction models must lead to increased interest in some of those previously unwanted inertial-gravity type waves especially as they affect mesoscale weather patterns in the midlatitudes and as they are present in the form of equatorial waves of mixed Rossby-gravity type. Forcing by heating may of course be involved for all these types of waves so therefore even the normal mode method of initialization may be limited and even more so near the equator, where the separation of the waves based on frequency is not feasible.

In the second part of the earlier work (1973b), the author did begin to consider the inclusion of mass forcing and friction into the dynamic initialization procedure using a global free surface model but the model was not only too crude, having only the 10 degree mesh length but also it did not have the best spatial staggering of points for the purpose of simulating geostrophic adjustment.

II. Model Experiments

The model used in this work is still the free surface primitive equation model. It describes an incompressible, homogeneous fluid with a flat lower boundary, a free upper surface and is subject to rotation. It is applied on a sphere. The finite difference equations are based on the energy conserving requirement proposed by Lorenz and applied and developed by Arakawa. They are written in momentum flux form thus,

$$\frac{\partial}{\partial t}\left(\frac{\phi u}{MN}\right) + \frac{\partial}{\partial \lambda}\left(\frac{\phi u}{N} u\right) + \frac{\partial}{\partial \varphi}\left(\frac{\phi v}{M} v\right) - \left[\frac{f}{MN} + \left(v \frac{\partial}{\partial \lambda}\frac{1}{N} - u \frac{\partial}{\partial \varphi}\frac{1}{M}\right)\right]\phi v = -\frac{\phi}{N}\frac{\partial \phi}{\partial \lambda} - K_f \phi u \qquad (1)$$

$$\frac{\partial}{\partial t}\left(\frac{\phi v}{MN}\right) + \frac{\partial}{\partial \lambda}\left(\frac{\phi u}{N} v\right) + \frac{\partial}{\partial \varphi}\left(\frac{\phi v}{M} v\right) + \left[\frac{f}{MN} + \left(v \frac{\partial}{\partial \lambda}\frac{1}{N} - u \frac{\partial}{\partial \varphi}\frac{1}{M}\right)\right]\phi u = -\frac{\phi}{N}\frac{\partial \phi}{\partial \varphi} - K_f \phi v \qquad (2)$$

$$\frac{\partial}{\partial t}\left(\frac{\phi}{MN}\right) + \frac{\partial}{\partial \lambda}\left(\frac{\phi u}{N}\right) + \frac{\partial}{\partial \varphi}\left(\frac{\phi v}{M}\right) = \mathcal{J} \qquad (3)$$

where $1/M = a \cos \varphi$; $1/N = a$ and $a \equiv$ radius of the earth, $\varphi \equiv$ latitude, $\lambda \equiv$ longitude, $\phi \equiv$ geopotential, $u \equiv$ zonal component of the wind, $v \equiv$ meridional component of the wind, $f \equiv$ coriolis parameter, $K_f \equiv$ is a Newtonian friction coefficient and $\mathcal{J}$ represents some as of yet unspecified source or sink of mass (a simulated "heating" or "cooling").

The finite difference equations are now written using the Arakawa scheme C (Winninghoff, 1968; Arakawa and Lamb, 1977) which is superior for describing geostrophic adjustment. For these experiments a 72 degree wide sector of the sphere is used and the increments of longitude and latitude are 4 degrees. A six minute time step is used. Therefore, because of the convergence of the meridions a Fourier smoothing of the zonal pressure gradient, the zonal convergence in equation 3, and the zonal components of the horizontal advection

in Eqs (1) and (2) is used (Arakawa, 1971), to satisfy the linear stability criterion. Though the leapfrog time step is normally used during the regular forecast runs, an Euler backward step is inserted every 5 time steps mainly to control any solution separation caused by use of mass source terms. During the initialization phase, to be explained later, only the Euler backward steps are used.

To review, during the dynamic initialization phase the model is integrated alternatively forward and backward for a few time steps until the fields of mass and wind appear to settle into near balance. It is during this procedure that the Euler backward scheme is used exclusively since it has damping effects on the high frequency motions. In addition, a constraint of the form

$$\alpha^{n+1} = \alpha_*^{n+1} - K_\alpha (\alpha_*^{n+1} - \alpha^o) \qquad (4)$$

can be applied to the u, v, or ϕ fields or all of them where the K_α's might be latitude dependent. (A variation could be to have the K_α's scale dependent explicitly. In the east-west direction Fourier analyses could be used while in the north-south direction some other technique would be needed.) Where $K_\alpha = 0$, $\alpha^{n+1} = \alpha_*^{n+1}$ and where $K_\alpha = 1$, $\alpha^{n+1} = \alpha^o$ which is the initial value. To give full flexibility K_α's are usually limited to a value no larger than about .5. This whole method is quite simple and allows the equations, in whatever form they are cast, to approach a consistent semi-balanced state through the internal adjustment process itself.

The foundation of much of the work reported on here is the theory of geostrophic adjustment. From that theory, an important parameter is obtained - the radius of deformation, $\sqrt{\phi}/f$, which is the important length scale parameter separating what can be considered large or small scale relative to the adjustment process. In Figure 1 is plotted the radius of deformation using $\phi = 9800$

m^2/sec^2 in the solid line. If a typical scale of a wave is defined as $L/2\pi$, note that not only are all scales of motion small near the equator, but even at 60 degrees waves of 6000 kilometers or less in wave length are not large and thus the winds are still an important source of initial data. In the model used here with a mesh size of 4 degrees $\Delta\lambda$ at 60 degrees is only 222 kilometers. So even a 18 $\Delta\lambda$ wave, the longest permitted, is about 4000 kilometers in length and is still small scale. In the earlier work a 10 degree mesh was used around the entire 360 degree circle so therefore, larger scale waves were possible at higher latitudes. The results there reflect this. The focus in this work will be directed more to the small scale because of the interest in the equatorial area. The broken line in Figure 1 shows the scale of the 18 $\Delta\lambda$ wave (longest permitted) in these calculations.

Experiment 1

Here the purpose was to verify and generalize the results given in the second half of 1973b for the "diabatic" type of initialization.

To begin, a control run was set up and run 84 hours. From the data generated 48 hours into that run, other runs were made using variations of dynamic initialization so that comparisons could be made of the new forecasts to the original control run. Usually the geopotential at some point was used for this purpose. The change in the free surface height is somewhat like the temperature fields in a baroclinic atmosphere and thus related to the vertical motions as well. Here, however, only the one external mode is involved.

The initial data for the control run was specified using

$$\phi^o = g[(1000 + 480 \cos\varphi) + (100 \sin\chi_1)\delta_1 + (150 \sin \mu\lambda\ \chi_2)\delta_2] \qquad (5)$$

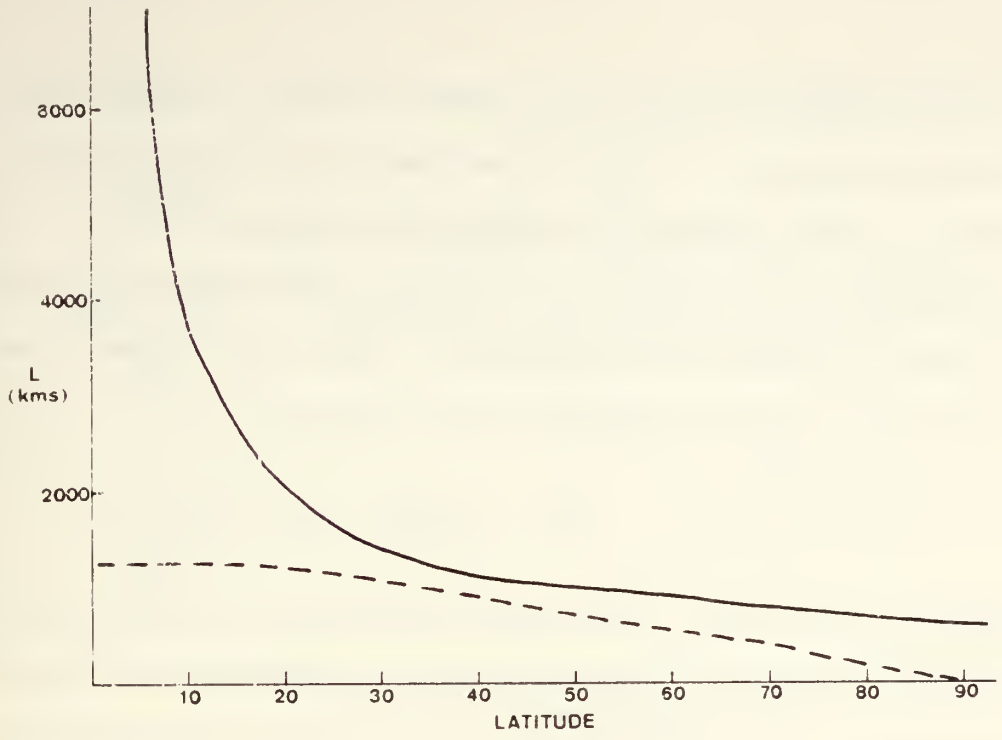

Figure 1. Radius of deformation as a function of latitude, $\bar{H} \approx 1000$ meters (solid line). Approximate scale of 18 Δ wave, the longest permitted (dashed line).

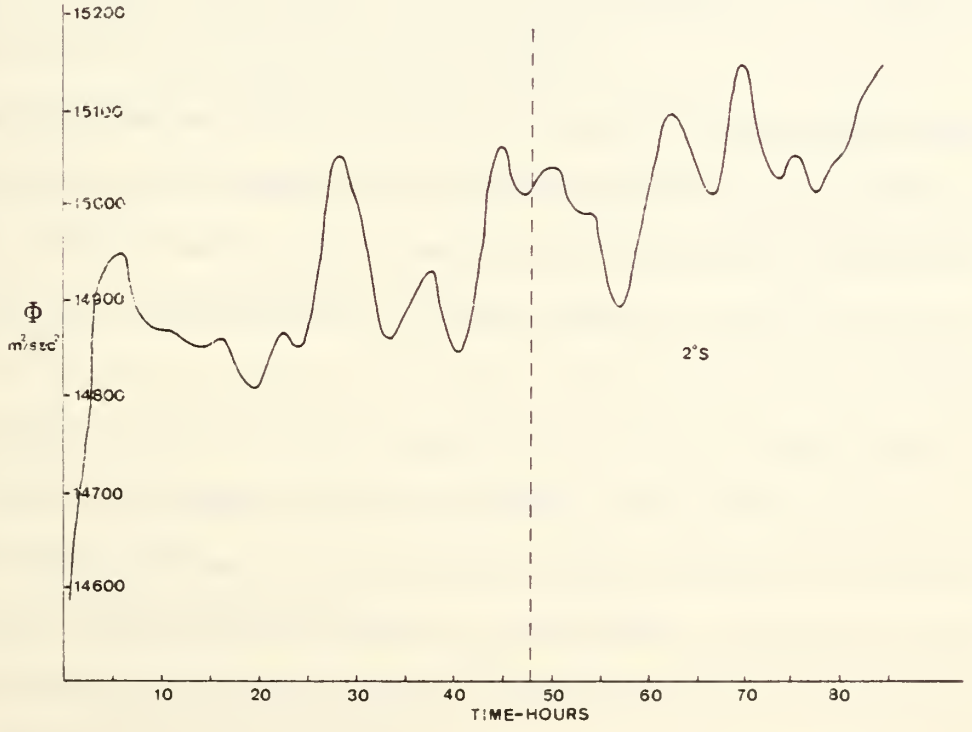

Figure 2. Temporal evolution of Φ at a selected point at 2^{o}S, 84 hour free run.

for the geopotential where ϕ^o is given in m^2/sec^2. Here φ is the latitude, λ is the longitude, μ is global wave number 5 (1 for the limited 72 degree wide grid), χ_1 and χ_2 are also latitude angles but are modified so that χ_1 runs from 0 to π for φ from $\pm$ 62 degrees to $\pm$ 2 degrees and χ_2 runs from 0 to π for φ from $\pm$ 62 degrees to $\pm$ 30 degrees. Outside these ranges δ_1 and δ_2 are 0. The initial velocity components are (in m/sec)

$$u^o = -\frac{\partial}{\partial\varphi}\left(\frac{\phi}{f_o}\right) , \quad v^o = \frac{\partial}{\partial\lambda}\left(\frac{\phi}{f_o}\right) , \tag{6}$$

where $f_o = 10^{-4}$ sec^{-1}. (5) gives a geopotential increasing into the tropics, but with a slight dip near the equator and allows for one wave in the middle latitudes. This run is initialized deliberately rather poorly in order to excite inertial-gravity waves of sigrificant amplitude. In addition, a mass source term is applied,

$$\mathcal{J}\phi = (0.5 - |\sin\varphi|)\phi^2\Delta t(.4^{-10}) \tag{7}$$

where $\mathcal{J}\phi$ is added to ϕ at each time step. This amounts to about .7 meters near the equator tapering off to 0 at 30 degrees N/S, and to a loss of about .7 meters near the poles. In addition, a point source of about 2 meters each time step is allowed at a point located at 2 degrees South near the middle of the grid.

Friction is included with $K_f = 3 \times 10^{-6}$. Figure 2 displays the value of ϕ at the point where the point mass source is applied and Figure 3 shows ϕ at a point at 46 degrees South. Note especially the phase and the amplitude of the inertial-gravity oscillations after hour 48. Amplitude seems to average about 10 meters or about 1 percent of the total depth and the two most prominent frequencies seem to be about one oscillation in 6 hours and one oscillation in

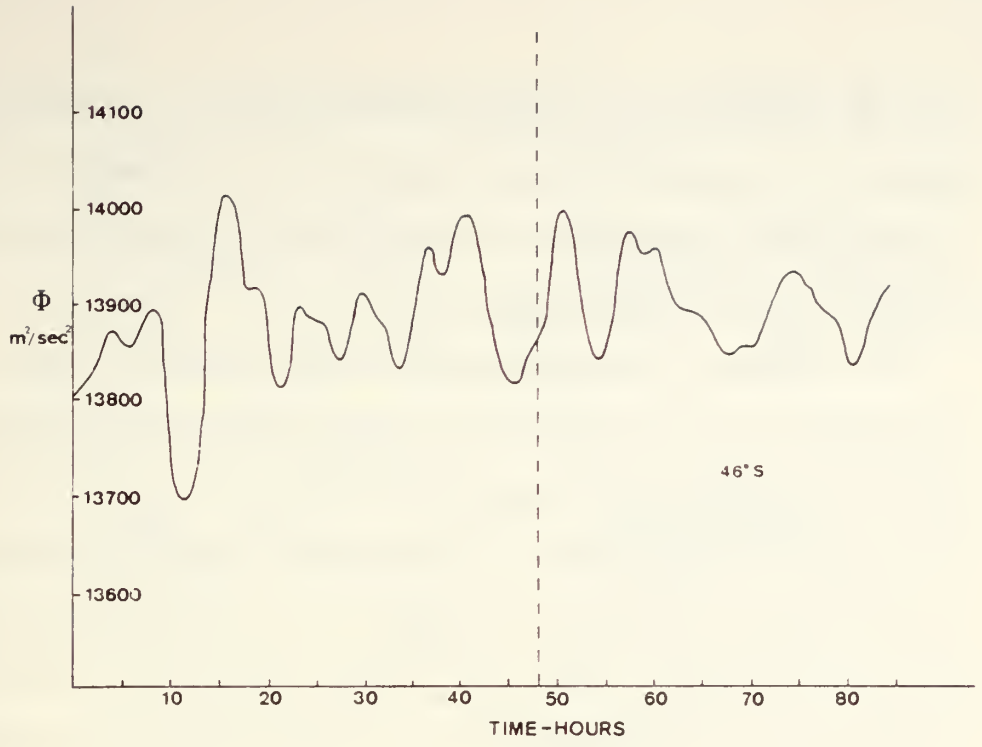

Figure 3. Temporal evoluation of Φ at a selected point at 46°S, 84 hour free run.

20 hours both near the equator and in the mid-latitudes. At 46 degrees however the amplitudes were reduced to near 5 meters.

Some physical understanding of why such waves are generated may be sought in examination of the initial conditions and the nature of the mass source which is a point mass source at 2°S. A harmonic analysis in the east-west direction does indicate a maxima in wave numbers 1, 2 and 4 in the ϕ field near the equator well into the forecast. These have wavelengths of about 8000, 4000 and 2000 kilometers respectively. If C, the phase speed of gravity waves near the equator is $\sqrt{\phi}$ this is $\sqrt{15000}$, or about 120 m/sec. The frequency P can be computed from L/C, so for wave numbers 2 and 4, P is approximately 9 hours and 4.5 hours, respectively. For wave number 1 it would be about 18 hours. In the initial conditions the second term in Eq (5) will give a wavelength of about 64° in the north-south direction (or ~ 7050 kms) and the point source term will excite waves of all lengths. So, to give an example at

hour 60, at 2°S where the mean ϕ is 14996 m^2/sec^2, the amplitude of wave number 1 is 44 m^2/sec^2, of wave number 2 is 11.8 m^2/sec^2, of wave number 3 is 1.32 m^2/sec^2, of wave number 4, 2.38 m^2/sec^2 and even of wave number 9 is .06 m^2/sec^2 which is insignificant.

Wave number 1 is predominant in the midlatitudes as well. Of course this comes from the third term in Eq. 5. Its length will vary from about 7000 kms at 30° to less than 4000 km above 60°. Here the computation of C should be from $\pm \sqrt{gH + f^2/K_L^2}$ since f is significant. Also its dimension in the y direction should be considered. Using 45° a value of C of about 140 m/sec is obtained. So here P ~ $(8.5 \times 10^6/140)^{sec}$ or 16 hours. Uncertainty in this computation is sufficient to make it also close enough to explain the longer observed period.

Next, consider the first term of Eq (5). The mean ϕ at 58° does show some indication of a very long oscillation. Its value rises to 12895.4 m^2/sec^2 at 24 hours, and then falls monotonically to 12743.2 m^2/sec^2 at 72 hours. The 82 hour run was not long enough to define the period completely but a 1/2 period of about 50 hours seems indicated. If the first term in Eq (5) is differentiated with respect to φ to obtain an expression for a mean $\bar{U}$ due to this term a value of about 5 m/sec is obtained $(480 (\sin \varphi)/f_o a)^*$. Again assuming a L_x of 4000 kilometers, P = 4,000,000 (m)/5(m/sec) or 800,000 sec which is of the order of 100 hours. This is the synoptic scale time variation.

Unfortunately the predominance of the shorter wave is not explained. It results probably from imbalances generated by the forcing, wave number interactions, and possibly difficulties generated near the poles (here wavelengths would be very short). The initial imbalance near the equator is quite large -

---

*a is the radius of earth ~6.3×10^6 m and f_o is 10^{-4} sec^{-1}.

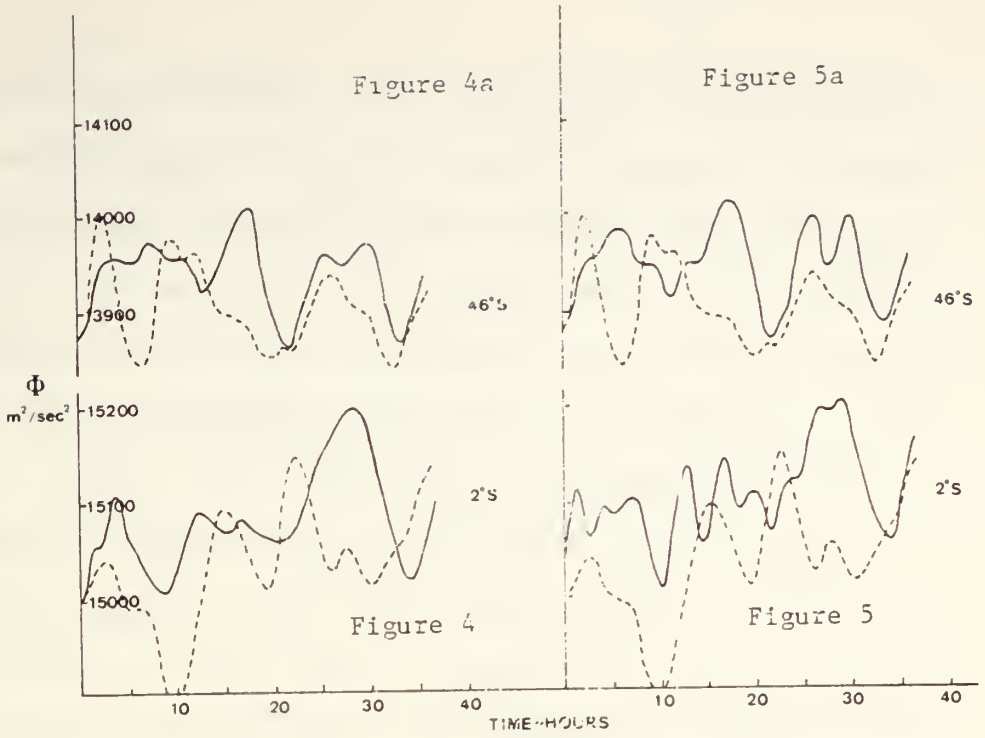

Figure 4. 36 hour forecast run, temporal evolution of ϕ at a selected point at 2^{o}S, initialized with semi-geostrophic wind (solid line), ϕ from last 36 hours of free run (dashed line). Figure 4a, same as Figure 4 for point at 46^{o}S. Initial ϕ in forecast run from free time.

Figure 5. Same as Figure 4 except ϕ replaced between 30^{o}S and 30^{o}N in the free run at hour 48 with a constant value of 15060 m^2/sec^2 to initialize the forecast run. Figure 5a, same as Figure 5 for point at 46^{o}S.

in fact the initial conditions were set up deliberately to generate noticeable noise.

Figures 4, 4a, 5, and 5a show the ϕ's evolution in time for a 36 hour prognostic control run initialized from data taken from 48 hours into the original 84 hour run. Figures 4 and 5 show the ϕ's at 2 degrees South, Figures 4a and 5a the ϕ's at 46 degrees South. Figures 4 and 4a are for a run where the winds were initialized from Eqs (6) and where the ϕ's were taken from the control run itself at 48 hours. Figures 5 and 5a are for a run where the ϕ at t=0 values for the forecast run between 30 degrees North and South were set at a constant value of 15050 m^2/sec^2. The winds again came from Eqs (6). For

comparison in the broken curves the ϕ values from the last 36 hours of the control run itself are plotted. Note the pattern of the noise. In neither run does the phase of any inertial gravity motion bear any resemblance to that indicated for the final 36 hours in Figures 2 and 3. Figures 4 and 4a are somewhat smoother. Note in Figures 4 and 5 the large amplitude wave at hour 27 1/2 and in Figures 4a and 5a the strong maxima at hour 17 1/2. There are no such oscillations in the broken curve.

Figures 6 and 6a show results at the same two grid points where dynamic initialization was carried out for 12 complete forward backward cycles and the cycle length was 12 time steps. No mass source or friction terms were used in the initialization but they were applied during the subsequent forecast. The K_α's of equation 4 were set at .5 for K_u and K_v from 30 degrees South to 30 degrees North, and K_h was set at 0 over this same range. North or south of these latitudes K_u and K_v varied linearly in latitude from .5 to .1 at the poles. This reflects the fact (see Figure 1) that even the longest waves permitted are still somewhat small scale in the mid-latitudes. In fact much testing of various values and distributions of the K's yielded the best results for the values above.

Comparison of the curves in Figures 6 and 6a to the broken curves now shows a very important result. To review, the reader is reminded that the tropical ϕ's were set to constant values at the beginning of the dynamic initialization. Unlike the previous results here the "real" inertial gravity motions are to some extent recovered. This is most striking in the phase of the waves though the amplitudes are not bad either. Still the amplitudes in the initialized run are definitely higher than the control run.

Next a considerable degree of testing of the incorporation of the mass source and friction terms into the dynamical initialization was carried out

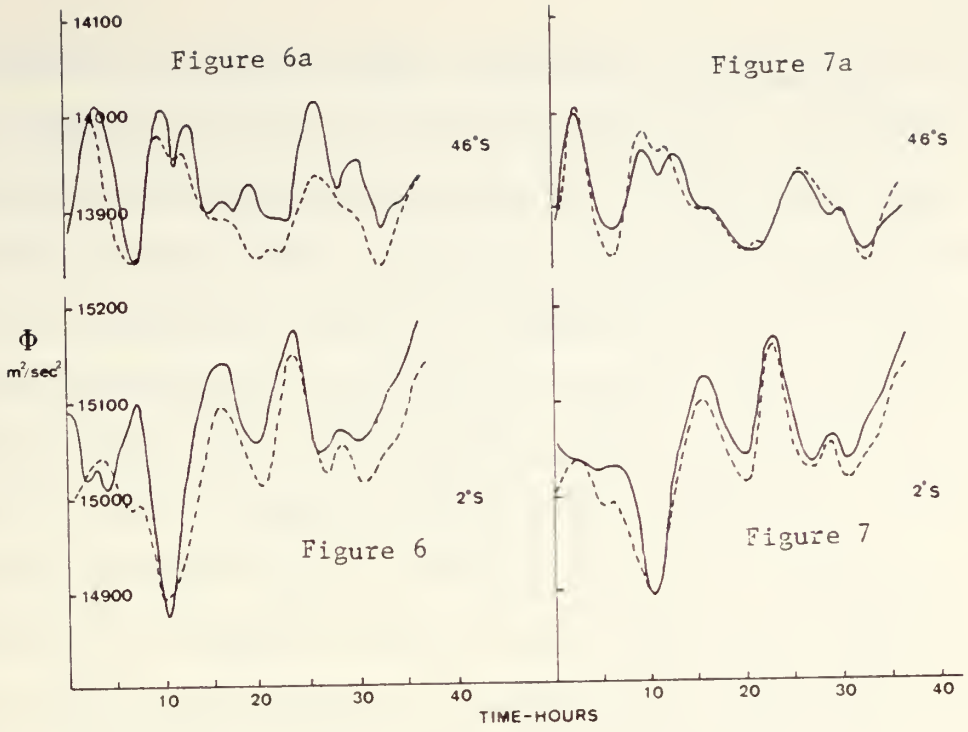

Figure 6. 36 hour forecast run, temporal evolution of Φ at a selected point at $2^{\circ}S$, adiabatic dynamic initialization (solid line), Φ from last 36 hours of free run (dashed line). Figure 6a, same as Figure 6 for point at $46^{\circ}S$.

Figure 7. 36 hour forecast run, temporal evolution of Φ at a selected point at $2^{\circ}S$, "diabatic" dynamic initialization (solid line), Φ from last 36 hours of free run (dashed line). Figure 7a, same as Figure 7 for point at $46^{\circ}S$.

much along the lines of that done in the earlier work (1973b). Here it was reestablished that the simplest procedure gave the best result. The mass source and friction terms, formulated exactly in the same manner as in the free run were allowed to operate only during the forward part of the cycle. Wind restoration was done during the entire cycle and the total wind was used throughout. It was found that this was superior to attempting to segment the wind into divergent and nondivergent parts and restore to one part or the other etc. (This may be due to computational difficulties of solving for such winds near the equator.)

An operational problem with this procedure is, of course, that the mass source and friction terms must be allowed only to operate on the tendencies of mass and wind but not to allow any accumulation or depletion of mass or energy during the initialization procedure. Merely requiring that zonal means stay constant is not sufficient (as in 1973b) as that cannot control the effects of the point source term. So what was done here was to aggregate the tendencies at each point due to the mass friction terms during the forward part of the cycle and then to subtract them out completely from u, v, and ϕ at the beginning of the backward part of the cycle. This is not quite the same as running these terms backward (formally possible in this somewhat artificial situation) as this would make no sense physically. Still this area may need further research to be applicable to a "real" atmosphere. At any rate, the results shown in Figures 7 and 7a are for this modified or diabatic initialization procedure. They show some improvement over the results in Figures 6 and 6a in the amplitudes. The phase is still well forecast and the amplitude is improved.

Some further tests were done discarding during the initialization some or all of the "real" mass values at points in the mid-latitudes. Recall from Figure 1 where it is suggested that even up to the poles these runs remain to some extent within the small scale range of motions though the 18 $\Delta\lambda$ wave is close to the radius of deformation. The results of these additional runs do indicate that some mass observations are needed. The case with no mass observations showed considerable deterioration again with respect to the amplitudes of the forecast inertial-gravity waves. Inclusion of some mass observations then moved the result almost linearly back toward that of Figure 7.

The importance of these results lies in the implication they have for tropical initialization at the present time and eventually for initialization

of mesoscale motions at all latitudes. Referring to the work of Matsuno (1966) as reviewed in Haltiner and Williams, pages 99-102, the dynamics of some potentially important equatorial waves are reviewed. That these may have profound effects under certain situations has been emphasized in Webster's studies. Though difficult to verify, this type of wave may have been responsible for the extremely heavy precipitation throughout central and southern California in January 1969. Thus in order to hope for any capability beyond the 4 to 6 day range with numerical models better initialization of Kelvin type and mixed Rossby-gravity type equatorial waves may be crucial.

Therefore several experiments were set up to examine the dynamical initialization procedure with respect to the larger scale in space (not relative to the radius of deformation) Kelvin and Rossby-gravity type waves First, the model was run 84 hours. The initial conditions were taken as a simple zonal flow with a maximum wind of 10 meters per second at the equator, no meridional flow, and the heights and winds in geostrophic balance via the linear balance equation. Here

$$\begin{aligned} u &= 10 \cos \varphi \text{(m/sec)} \\ v &= 0.0 \quad \text{(m/sec)} \\ \phi &= \phi_M + a^2\left[\frac{10}{2a}\left(2\Omega + \frac{10}{a}\right)\right] \cos^2 \varphi (\text{m}^2/\text{sec}^2) \end{aligned} \tag{8}$$

where $\phi_M = 5400 \times 9.81$ m^2/sec^2, a ≡ radius of the earth (6.375×10^6 m), $2\Omega \equiv 14.548 \times 10^{-5}$ sec^{-1}, φ is latitude in radians.

A Kelvin wave is generated by means of a simulated mass source term. It is of the form,

$$H = A \sin(\mu\lambda) \cos\left(\frac{\pi}{2} Y\right) \tag{9}$$

where A = 25 m^2/sec, $\mu = 2\pi/L$ (where L is set for wave number 1 for the

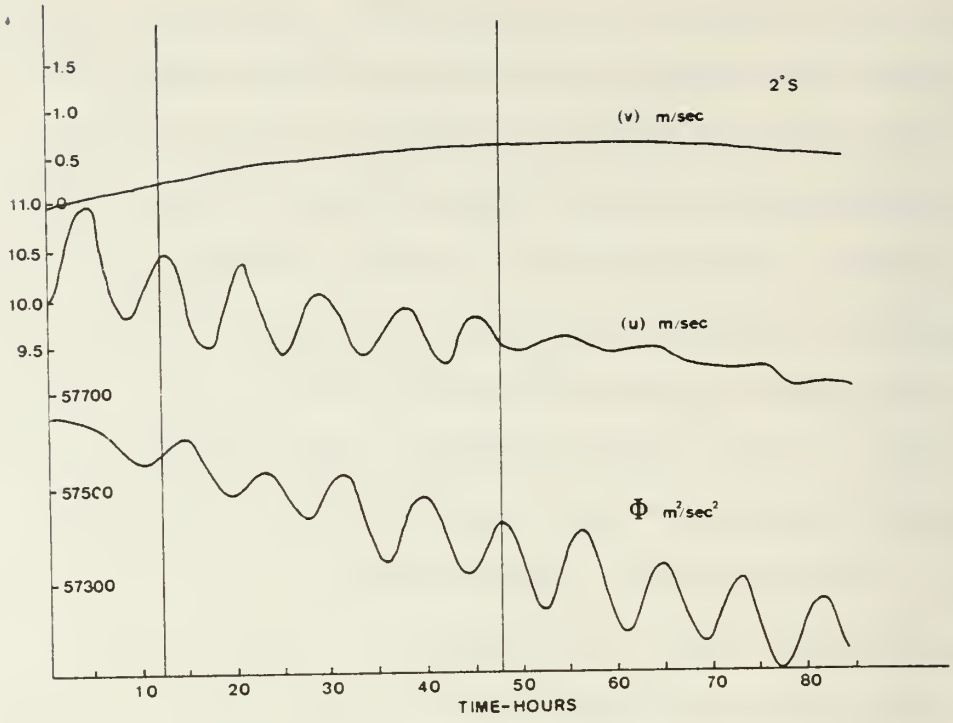

Figure 8. Free run with forced Kelvin wave, temporal evolution of Φ, U, V at selected points near each other in C scheme at 2^{o}S (V on equator).

model's grid which would correspond to wave number 5 for the globe), and Y is a linear function ranging from -1 to 1 between 30 degrees South and 30 degrees North. H is set equal to 0 in the mid-latitudes. Friction is allowed using the same formulation as earlier. In this case the mass source is stationary and is imposed on a zonal current.

In the remaining figures (8 through 25a,b,c) what is shown is first a plot with time at the point at 2 degrees South of the u, v, and Φ values and then maps of the u, v, and ϕ fields with some analyses made near the equator.

For the first 84 hour run which generates a Kelvin wave, Figure 8 displays the temporal plot of u, v and ϕ and Figures 9a,b,c show the field maps at 12 hours into the run. Figures 10a,b,c then show the field maps 36 hours later at 48 hours.

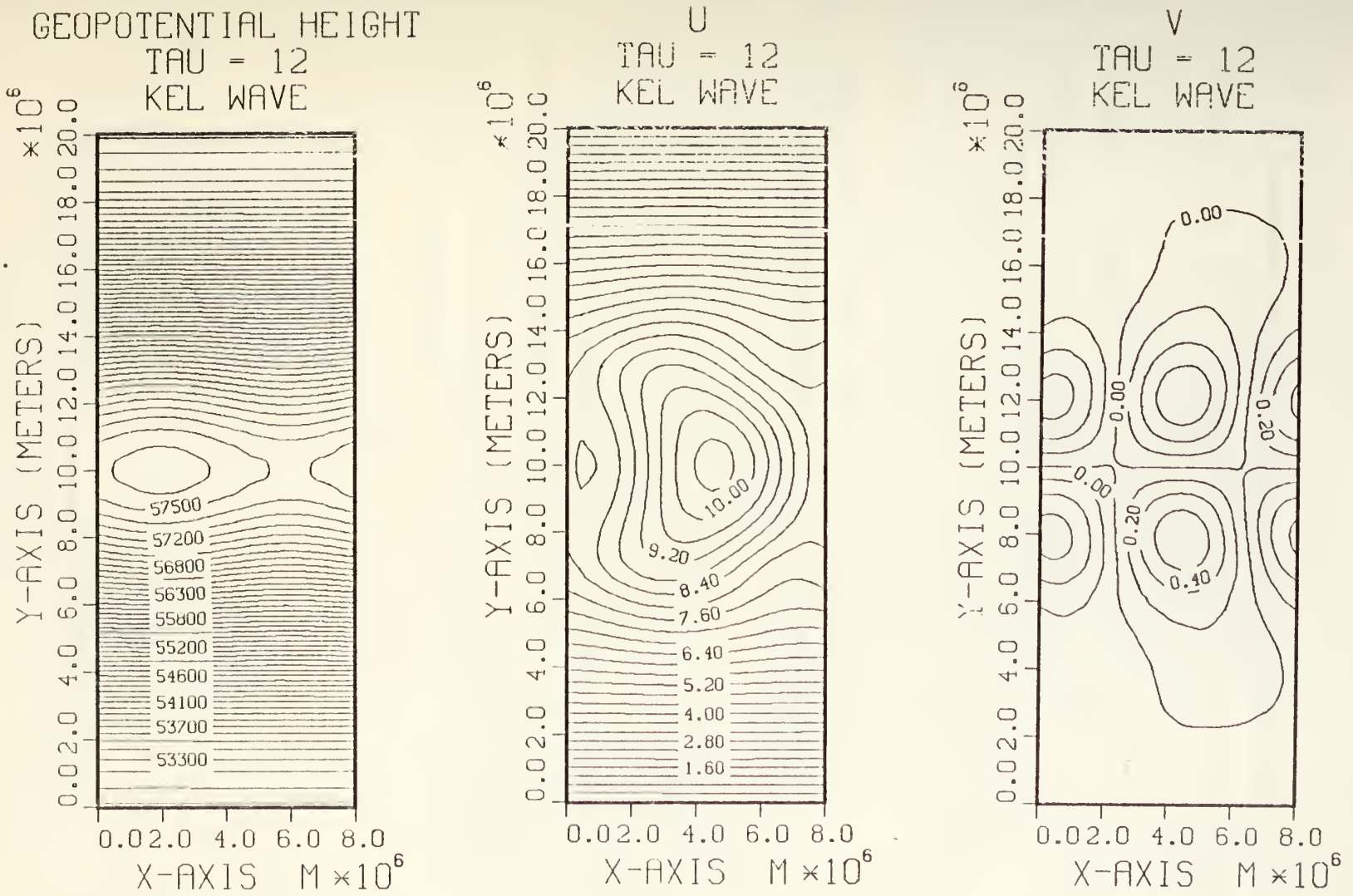

Figure 9. Free run with forced Kelvin wave. Spatial maps of Φ (Figure 9a), U (Figure 9b) and V (Figure 9c) at hour 12.

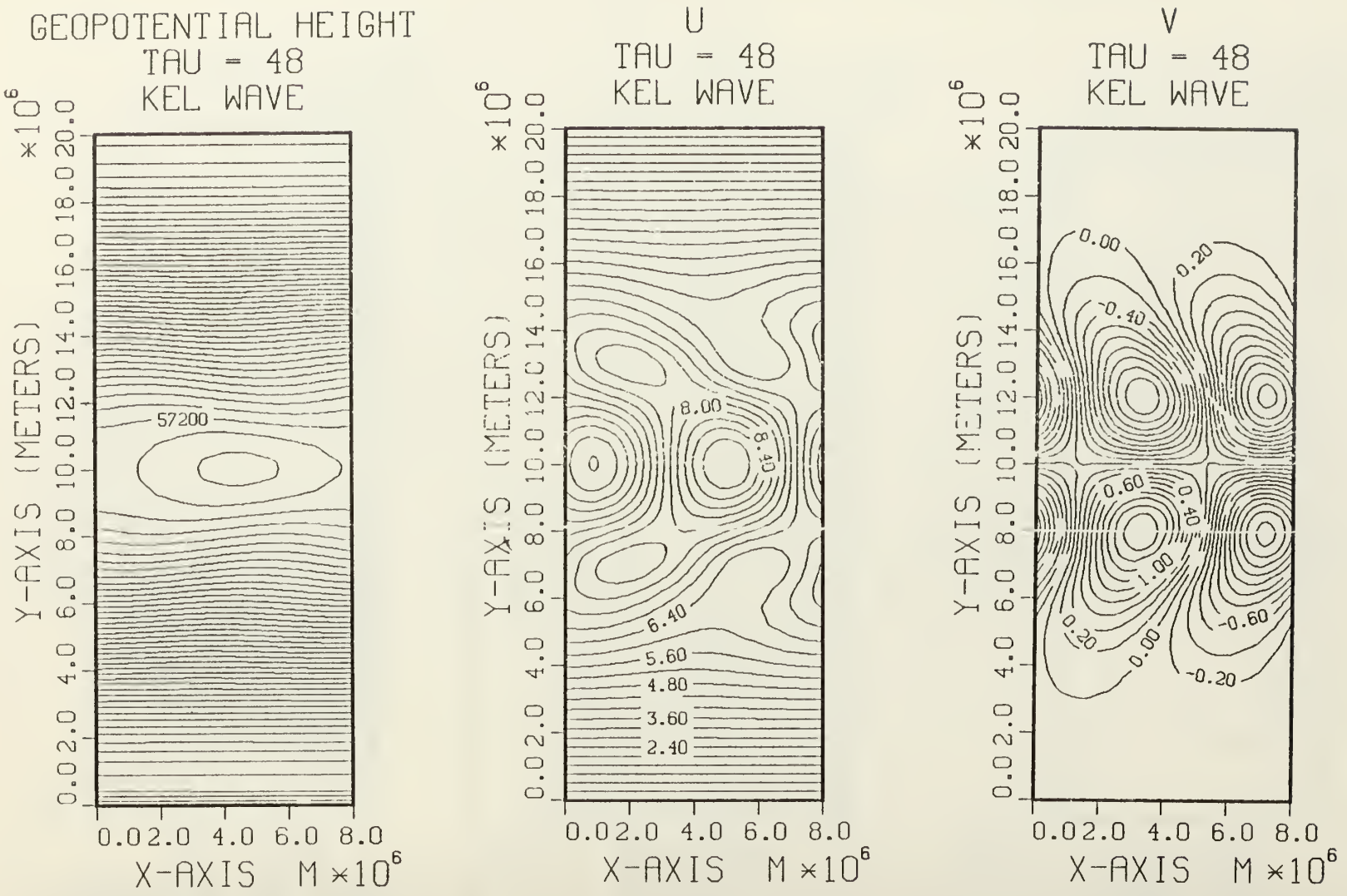

Figure 10. 10a, 10b and 10c, same as in Figures 9a, 9b, 9c except at hour 48.

Next an initialization-forecast run was made. The wind data were taken from the data at 12 hours into the free run. Heights in the tropics were replaced by a constant value (admittedly near the mean of the "real" data) and a "diabatic" type of initialization was done using 24 complete forward backward cycles (as in the case of Figures 7 and 7a). For this run the results are displayed in Figure 11, Figures 12a,b,c, and Figures 13a,b,c. Figure 11 is analogous to Figure 8, Figures 9a,b,c are analogous to Figures 12a,b,c and Figures 10a,b,c are analogous to Figures 13a,b,c. These results clearly show that the recovery of the mass field by the initialization and the subsequent forecast are quite remarkable. Note that some information regarding the tropical mass field was needed, if only just its mean value. The procedure can work with widely divergent values of the original (to the process) mass, but the results will not be very useful.

The remainder of the figures (14 through 25a,b,c show results from a group of runs in which Rossby-gravity type waves were involved. In these cases all or some of the initial fields were specified analytically and no mass source or friction terms were used. Specifically, for the first runs for which results are given in Figures 14, 15a,b,c, and 16a,b,c the initial u, v and Φ fields were specified from,

$$v = A \sin \mu\lambda \; e^{-\zeta^2/2} \tag{10}$$

$$u = Ky \; A \cos \mu\lambda \; e^{-\zeta^2/2} \tag{11}$$

$$\phi = - \left[\frac{\beta y}{\mu} + \frac{\nu}{\mu} Ky\right] A \cos \mu\lambda \; e^{-\zeta^2/2} + \Phi \tag{12}$$

where $\mu = \frac{2\pi}{L}$, $L = 18\ \Delta\lambda$, $A = 10$ m/sec, $\zeta = \sqrt{\beta y/\Phi^{1/4}}$, $\Phi \equiv 9.81 \times 5400\ m^2/sec^2$, $\beta = \frac{2\Omega}{a}$, $K = (B - \frac{\mu}{\nu} \Phi C_1^2)/(\frac{\mu^2}{\nu} \Phi - \nu)$, $C_1 = \zeta/y$, $\nu = \Phi^{1/4} \sqrt{\beta}(- \frac{k}{2} + \sqrt{\frac{k^2}{2} + 1})$ and $k = \frac{2\pi}{L} \sqrt{\beta}\ \Phi^{1/4}$. Here y=0 at the equator and is $\pm$ the distance in meters from

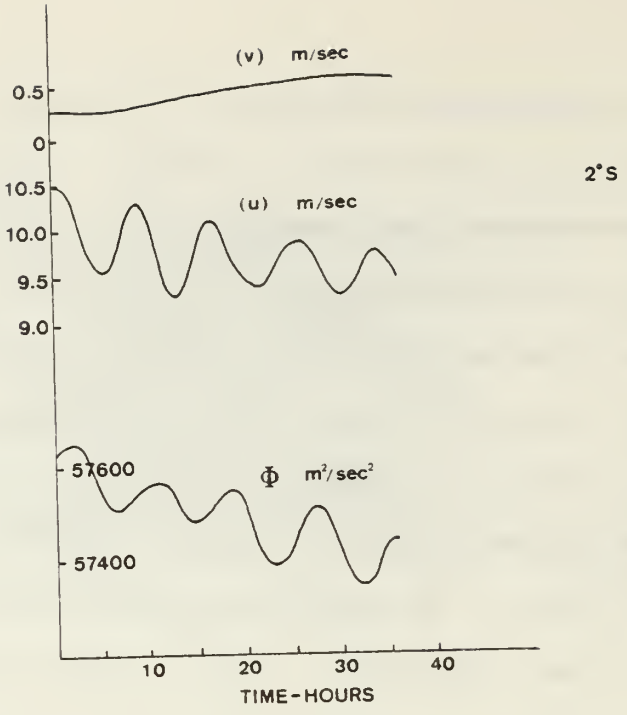

Figure 11. Forecast run with forced Kelvin wave, temporal evolution of Φ, U, V at selected points near each other in C scheme at 2°S (V on equator), "diabatic" dynamic initialization.

the equator respectively. These relations either come from or can be derived from those given in Haltiner and Williams, page 100, following the original work of Matsuno (1966). Figure 14 again displays the temporal evolution of u, v, ϕ at the point at 2 degrees South and Figures 15a,b,c and 16a,b,c are the field maps at hours 0 and 36 respectively.

Next, a run was made in which only the wind fields were initially specified from Eqs (10) and (11), but in which the Φ field would be generated by the adiabatic dynamical initialization procedure. Then a 36 hour forecast could be made using these fields. Figures 17, 18a,b,c and 19a,b,c show the analogous data for this run to that shown in Figures 14 to 16. Again the initialization recaptures the mass field quite well. In fact the total amplitude of the mass wave computed from Eq (12) (Figure 15c) is slightly greater than that from the initialization (Figure 17c).

Finally, a forecast type of experiment was done for the Rossby-gravity type wave as was done before for the Kelvin wave situation and the earlier cases.

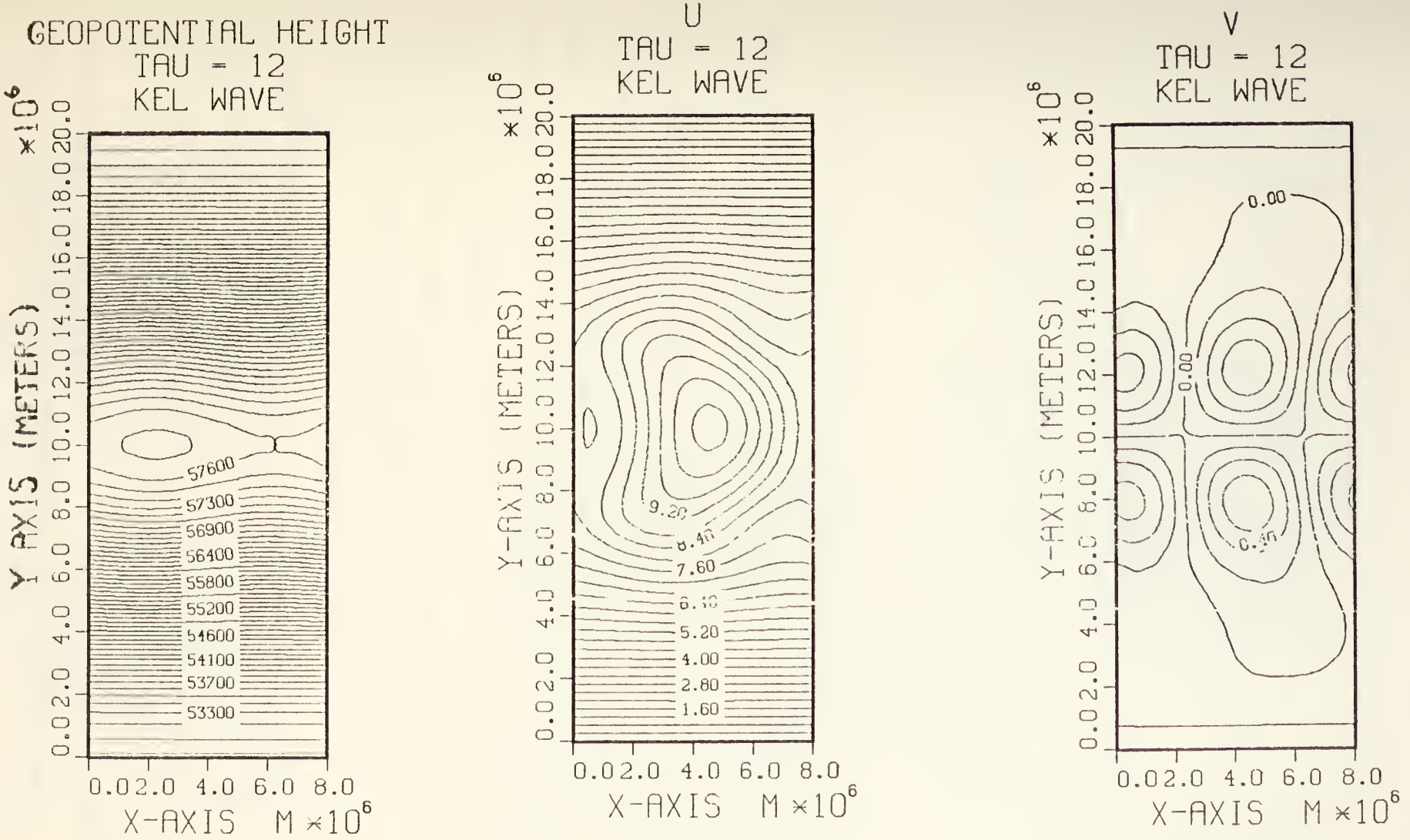

Figure 12. Forecast run with forced Kelvin wave. Spatial maps of Φ (Figure 12a), U (Figure 12b), and V (Figure 12c) after initialization. Wind data from hour 12 in free run used.

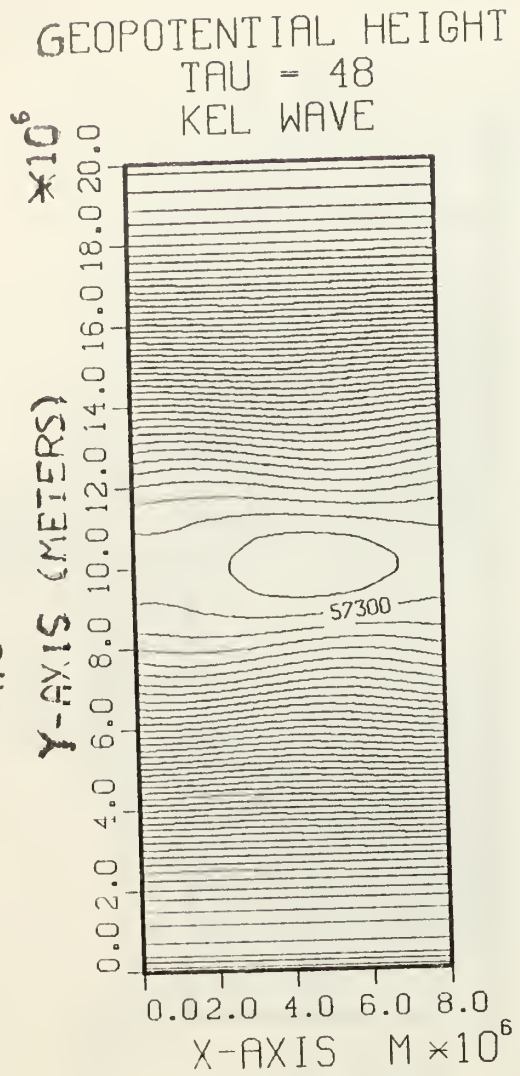

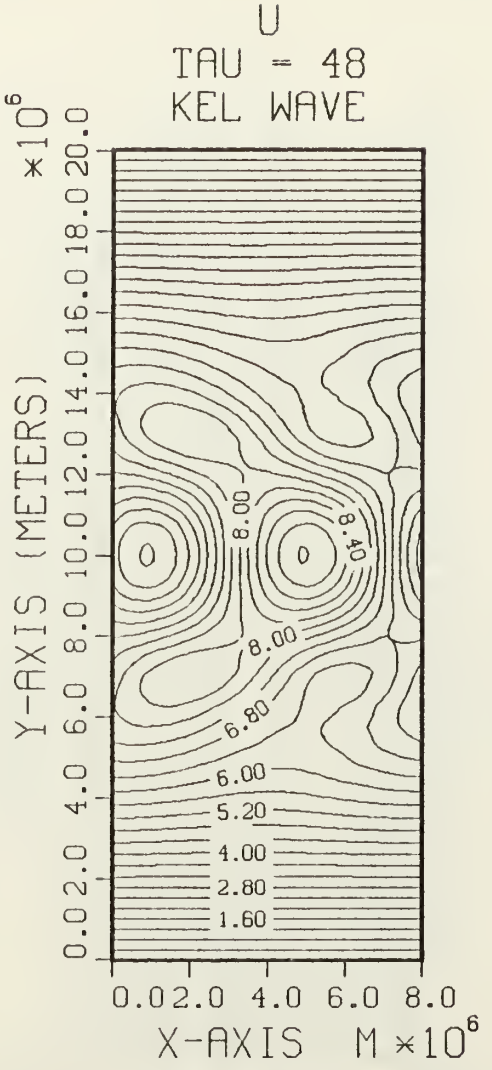

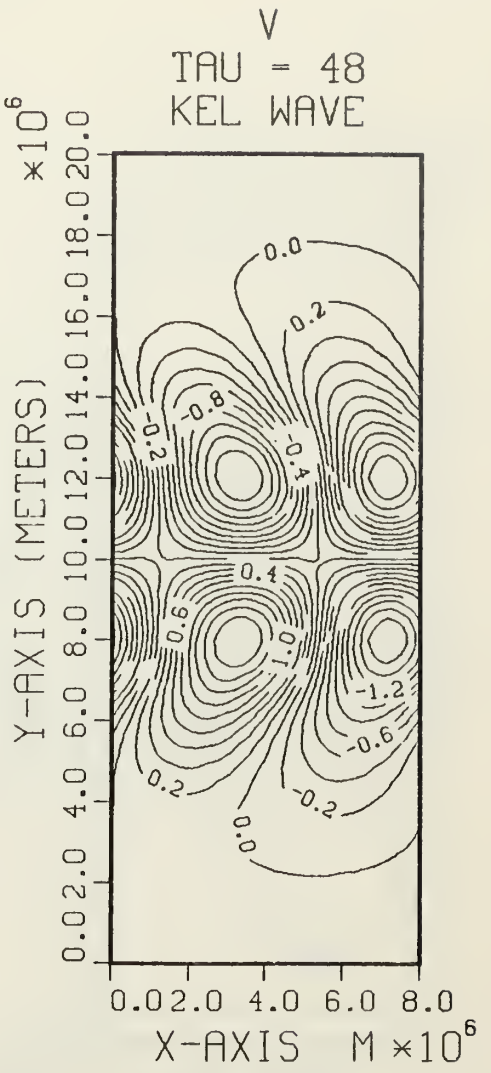

Figure 13. 13a, 13b, 13c, same as in Figures 12a, 12b, 12c but for 36 hours into forecast run.

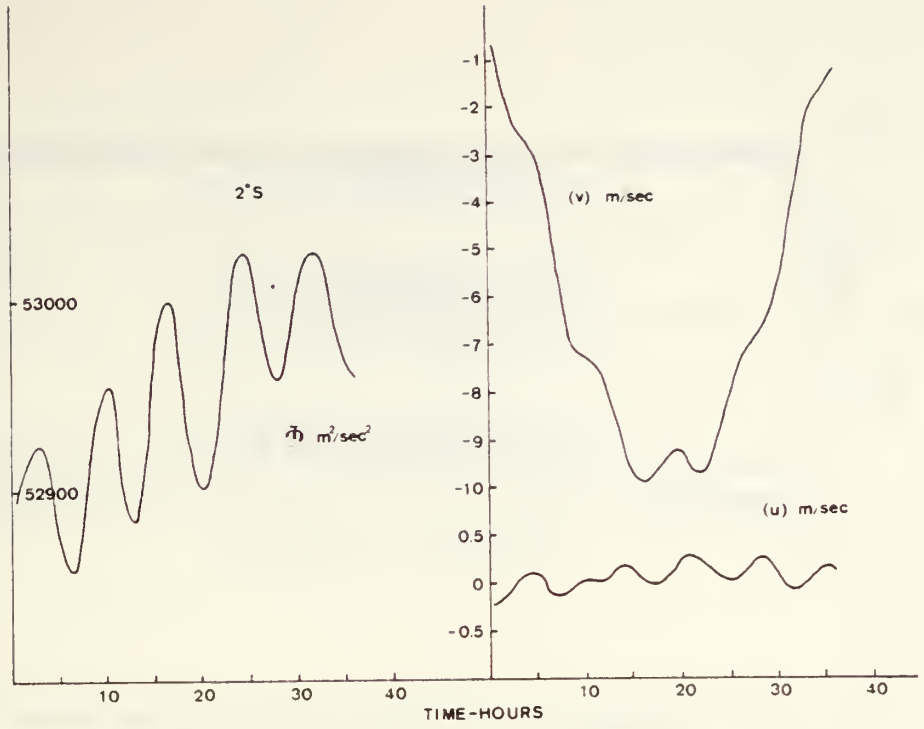

Figure 14. Free run, Rossby-gravity wave, temporal evolution of ϕ, U, V. Fields initialized analytically.

So the model, using all the Eqs (10)-(12) to start the run, was integrated for 84 hours. The data at hour 48 were stored so a reinitialization of the ϕ field could be done at that point and a 36 hour forecast could be made from that data. Figures 20, 21a,b,c and 22a,b,c show results from the free run with the field maps shown for hour 48 and hour 84. Finally Figures 23, 24a,b,c and 25a,b,c show the results for the forecast run with the field maps shown at the termination of the initialization and at 36 hours.

It is of special interest to compare the ϕ field in Figure 21c and the ϕ fields shown in Figure 24c. The field in Figure 21c is a "snapshot" of the ϕ field at hour 48 in the regular free run. To initialize the "forecast" run the u and v fields at hour 48 (Figures 21a, 21b) were retained, a constant value for ϕ from 30°N to 30°S was prescribed, and the initialization procedure was started. By its termination the ϕ field in Figure 24c was generated. The highest and lowest values are recaptured to within about 15 meters. The 36

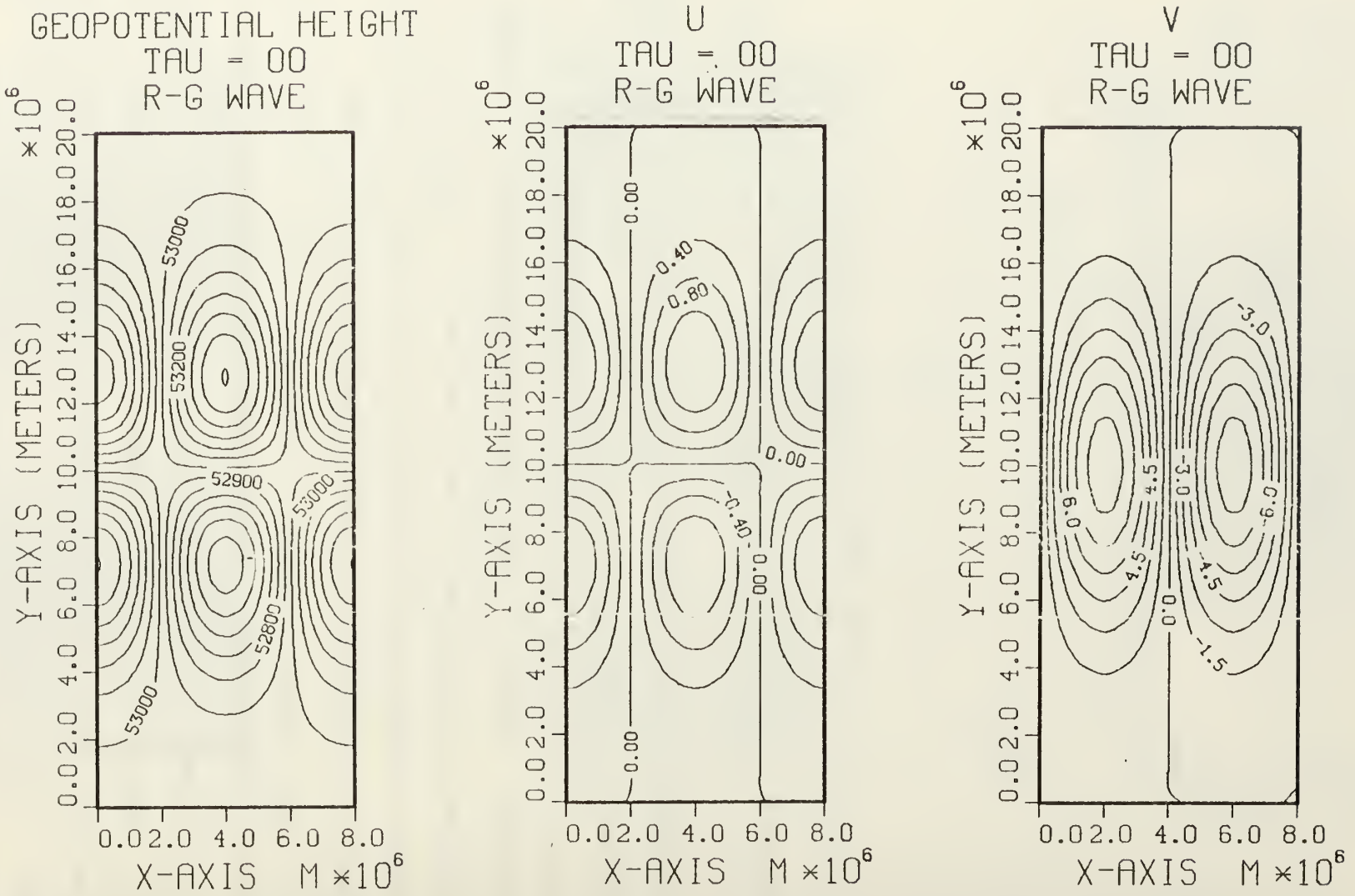

Figure 15. Free run, Rossby-gravity wave. Spatial maps of Φ (Figure 15a), U (Figure 15b), and V (Figure 15c). Hour 0, fields obtained analytically.

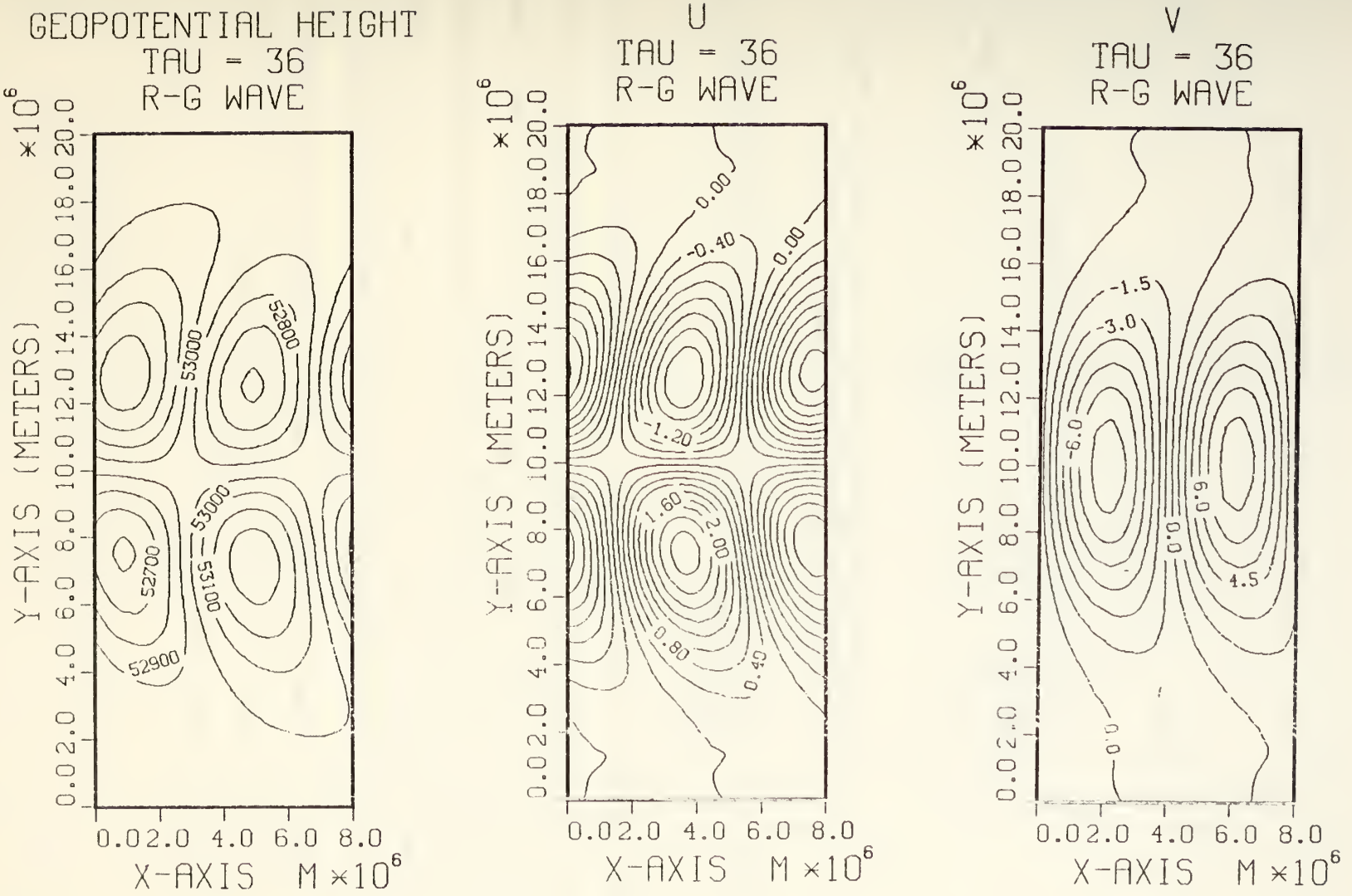

Figure 16. 16a, 16b, 16c, same as in Figures 15a, 15b, 15c except hour 36.

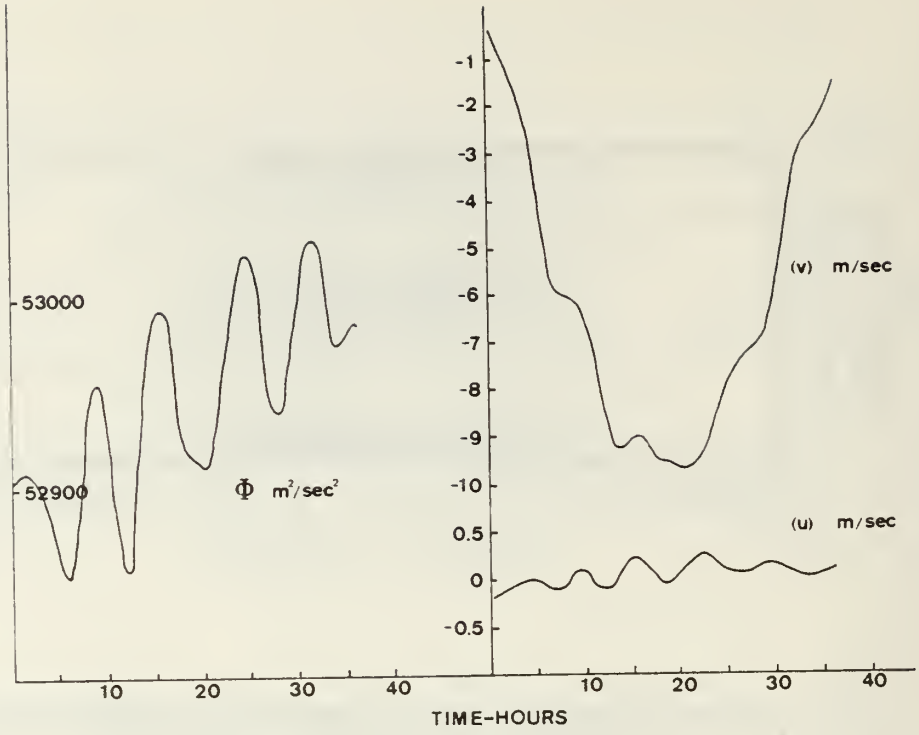

Figure 17. Free run, Rossby-gravity wave, temporal evolution of Φ, U, V. Initial winds obtained analytically. Initial Φ's from dynamic initialization.

hour forecast ϕ field (Figure 25c) is then to be compared to the 84 hour ϕ value in the control or free run (Figure 22c). Now the high and low centers are within 10 meters. Thus this method of initialization shows promise in capturing a difficult class of wave motions which may be of great importance in the atmosphere and which cannot be recaptured easily by any balancing type procedure - at least right near the equator. These waves may have an effect on NWP models namely; the need to observe and initialize them properly may be absolutely imperative in order to increase large scale predictability in the atmosphere beyond 4 or 5 days.

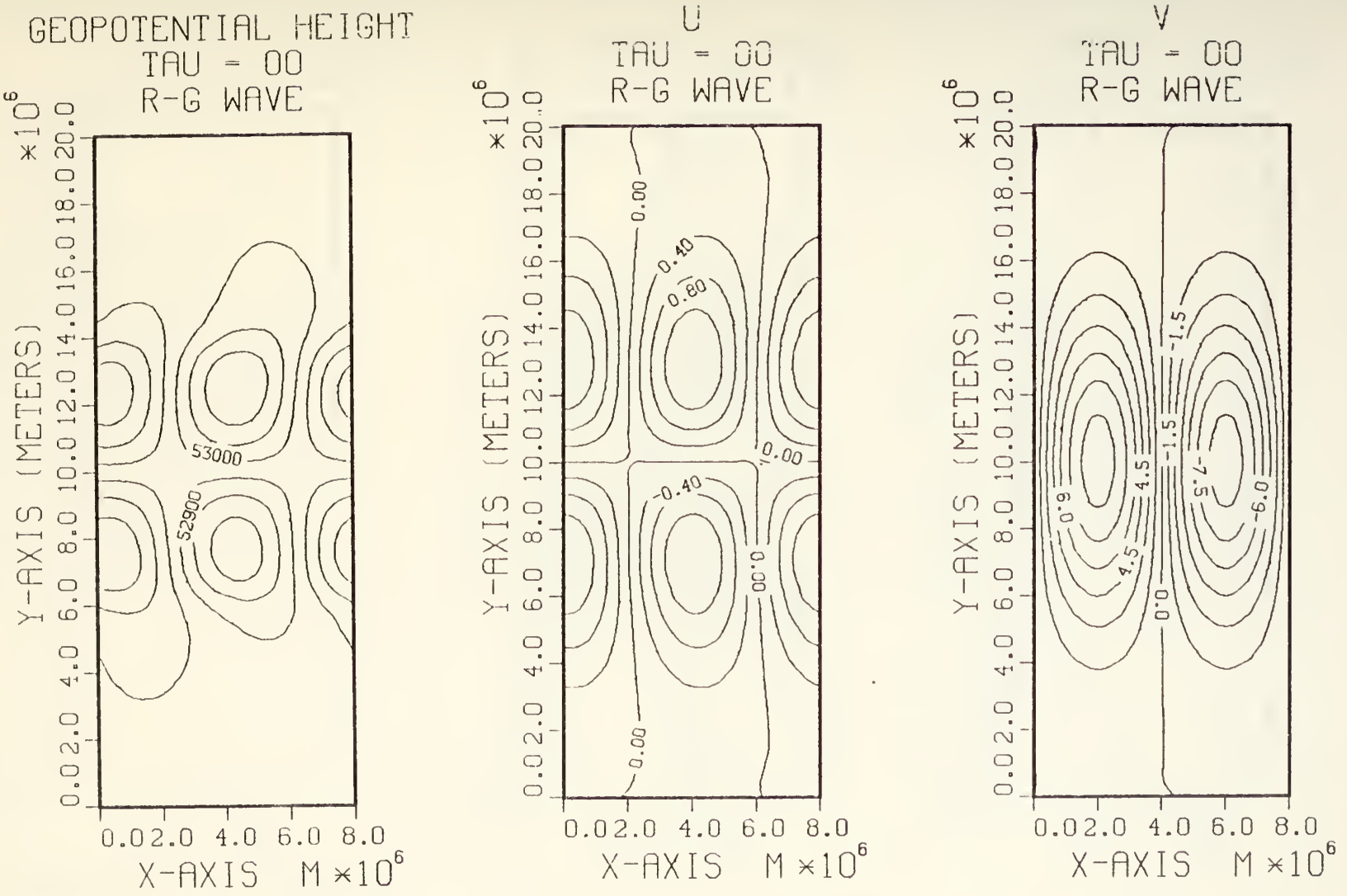

Figure 18. Free run, Rossby-gravity wave. Spatial maps of Φ (Figure 18a), U (Figure 18b), and V (Figure 18c). Hour 0, wind fields obtained analytically. ϕ field obtained from dynamic initialization.

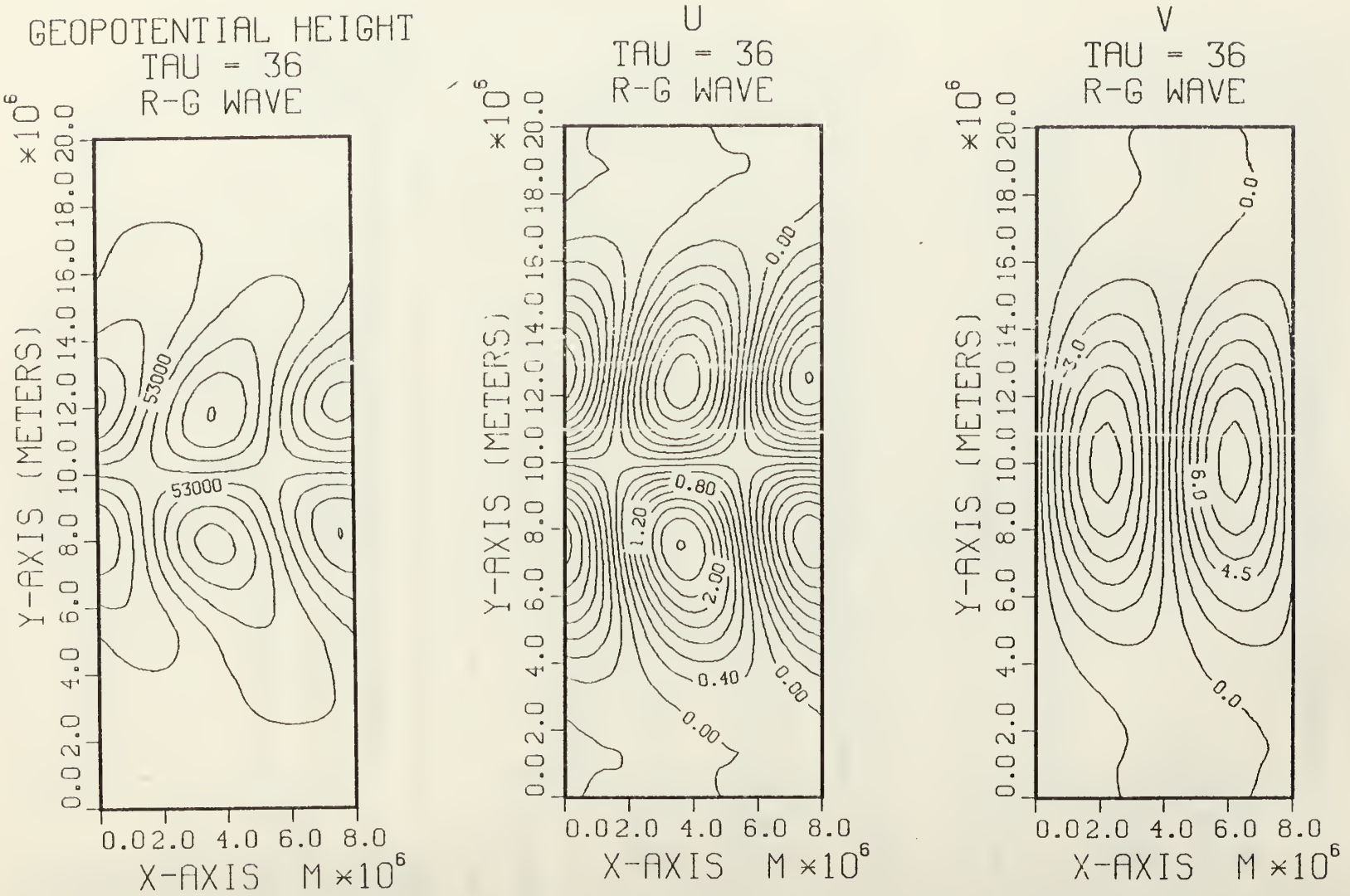

Figure 19. 19a, 19b, 19c, same as in Figures 18a, 18b, 18c except hour 36.

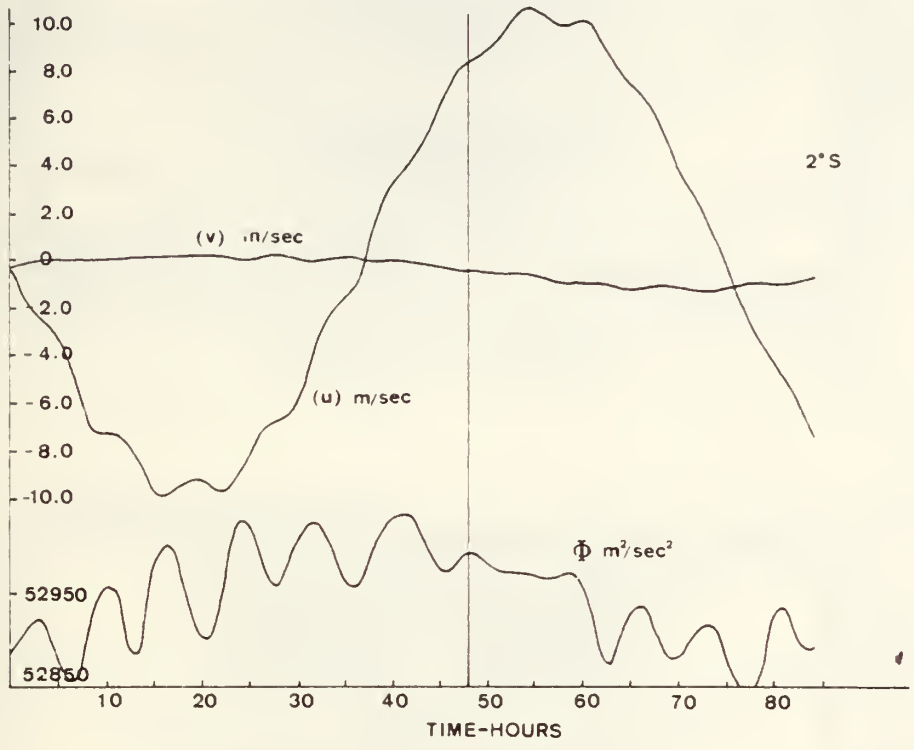

Figure 20. Same as Figure 14 but for long (84 hour) free run.

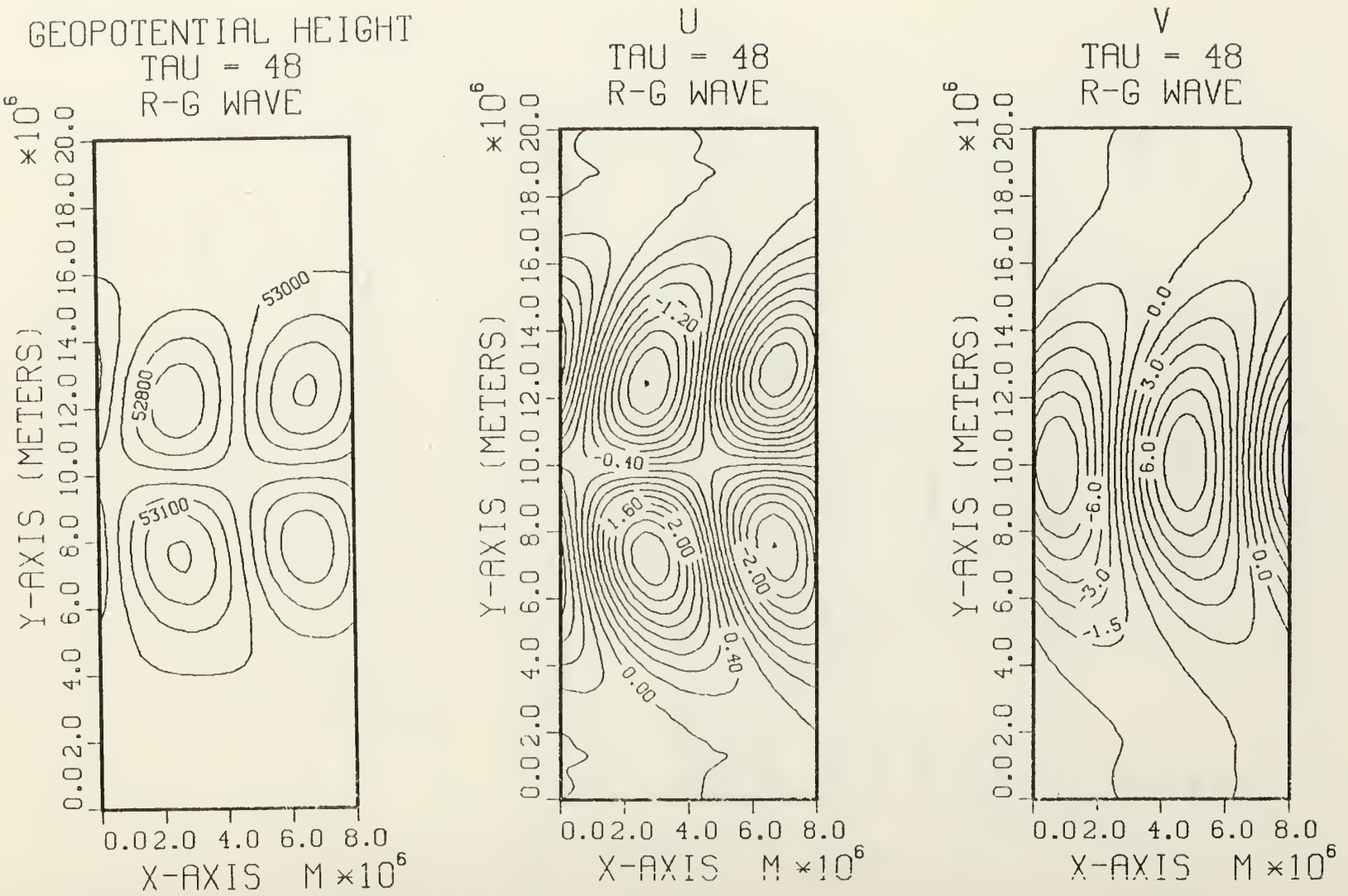

Figure 21. Long free run. Spatial maps of Φ (Figure 21a), U (Figure 21b), and V (Figure 21c). Hour 48 into long free run.

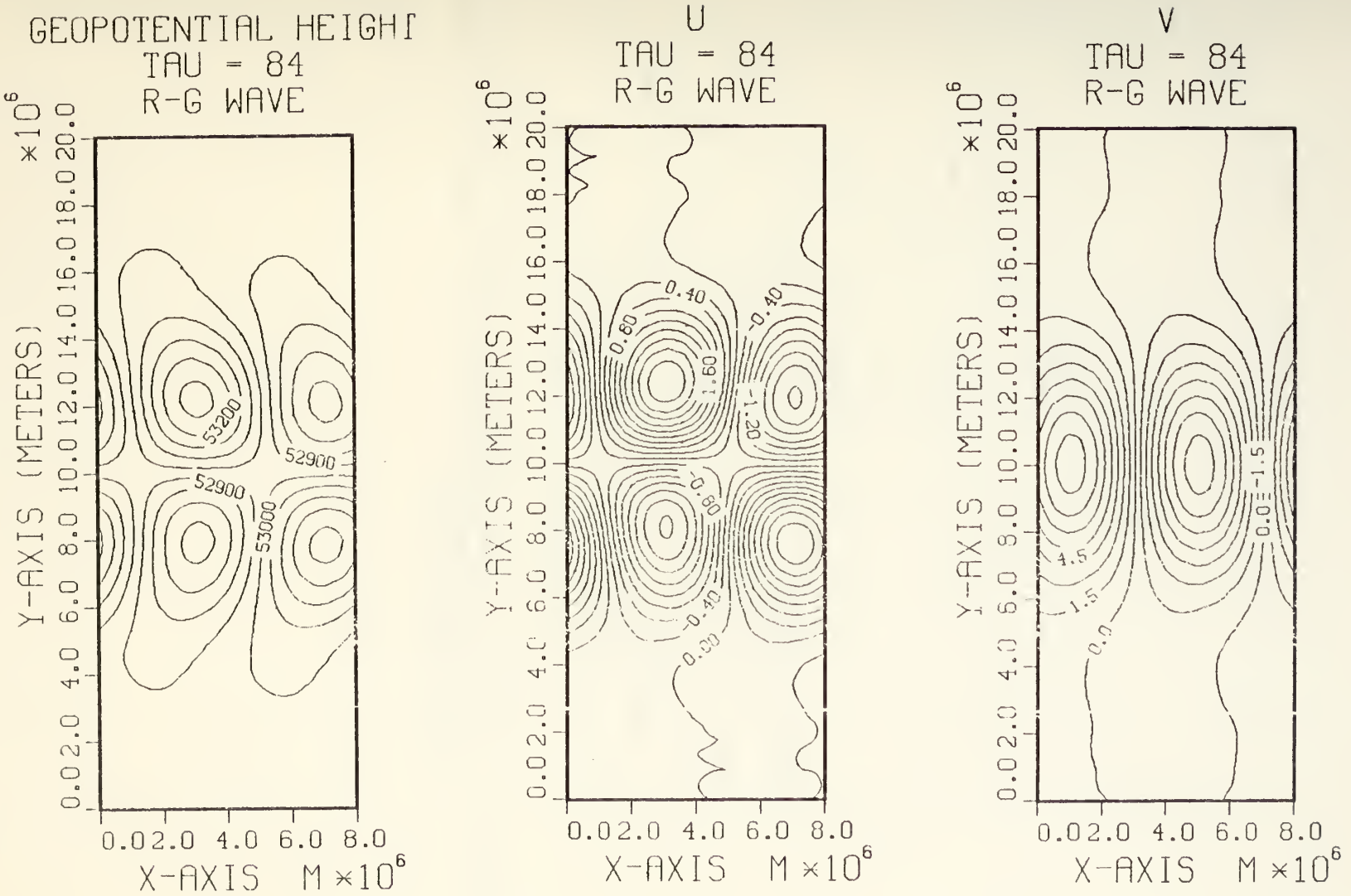

Figure 22. 22a, 22b, 22c, same as Figures 21a, 21b, 21c except at hour 84 into long free run.

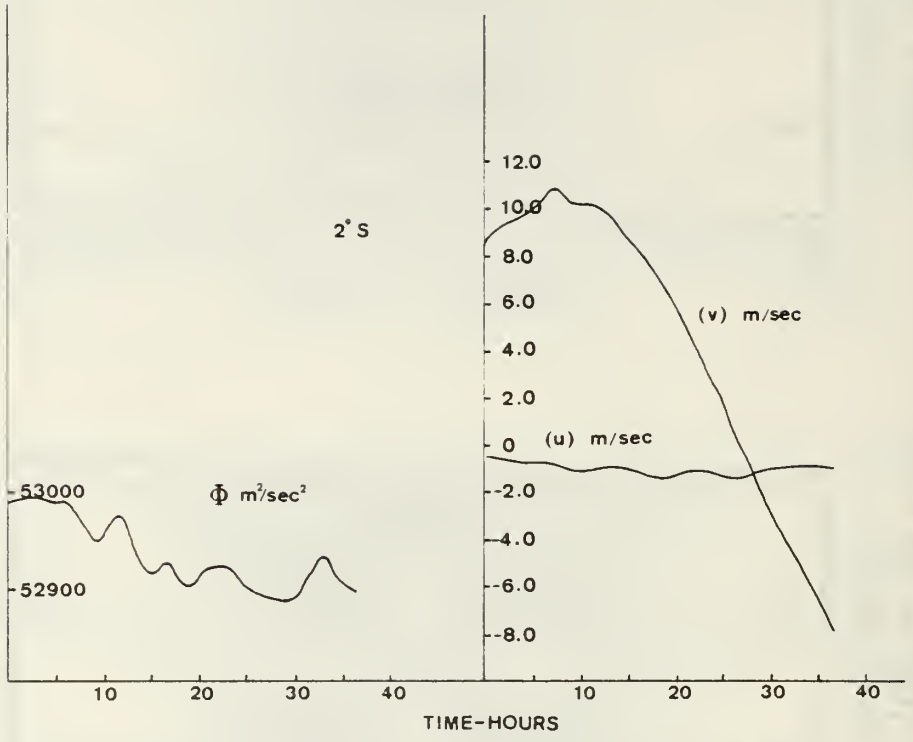

Figure 23. Forecast run, Rossby-gravity wave, temporal evolution of ϕ, U, V. Initial winds from hour 48 of free run. Initial ϕ's obtained from dynamic initialization.

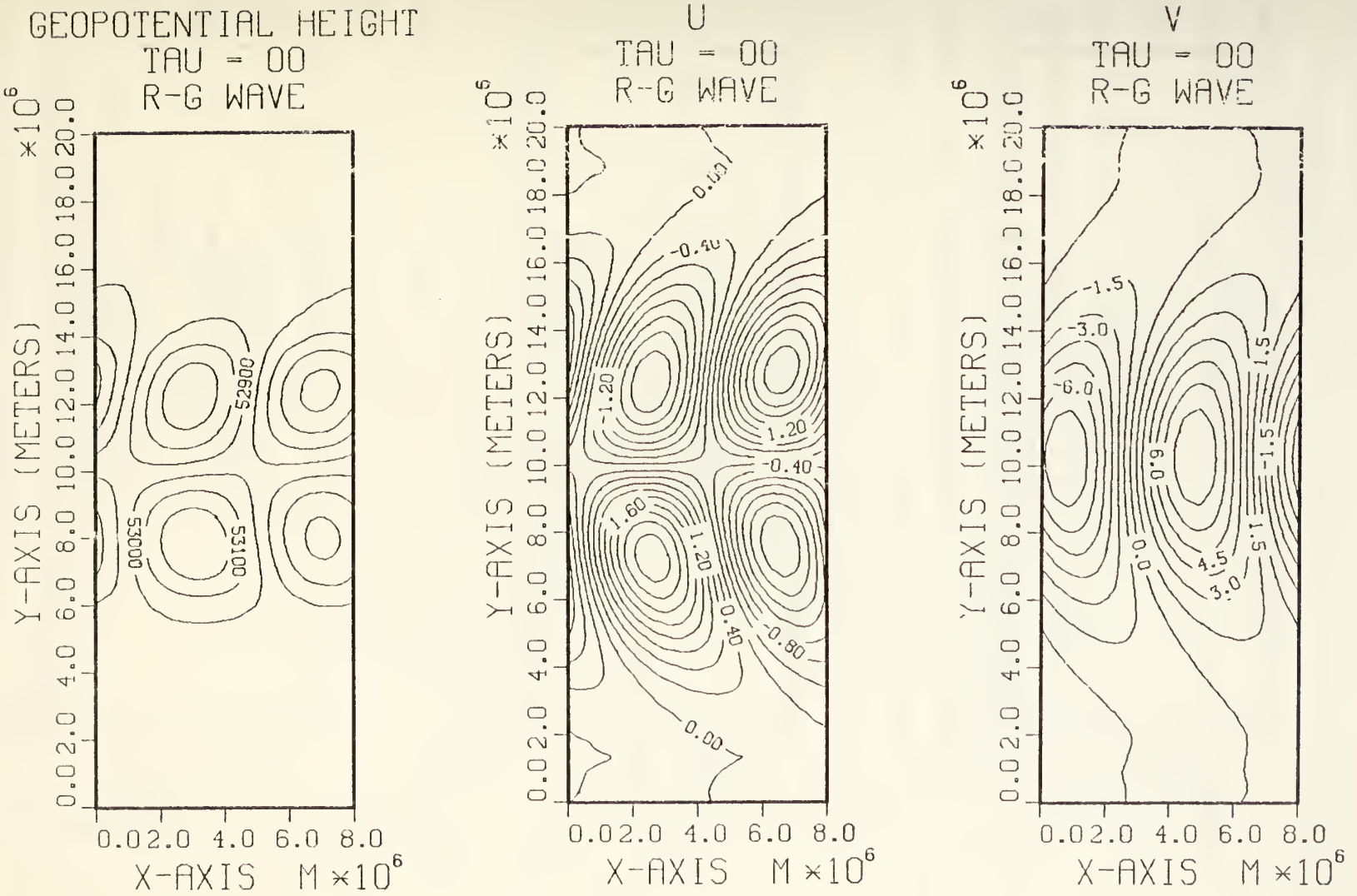

Figure 24. Forecast run, Rossby-gravity wave. Spatial maps of Φ (Figure 24a), U (Figure 24b), and V (Figure 24c). Hour 0 of forecast run. Winds from hour 48 of free run, ϕ's obtained from dynamic initialization.

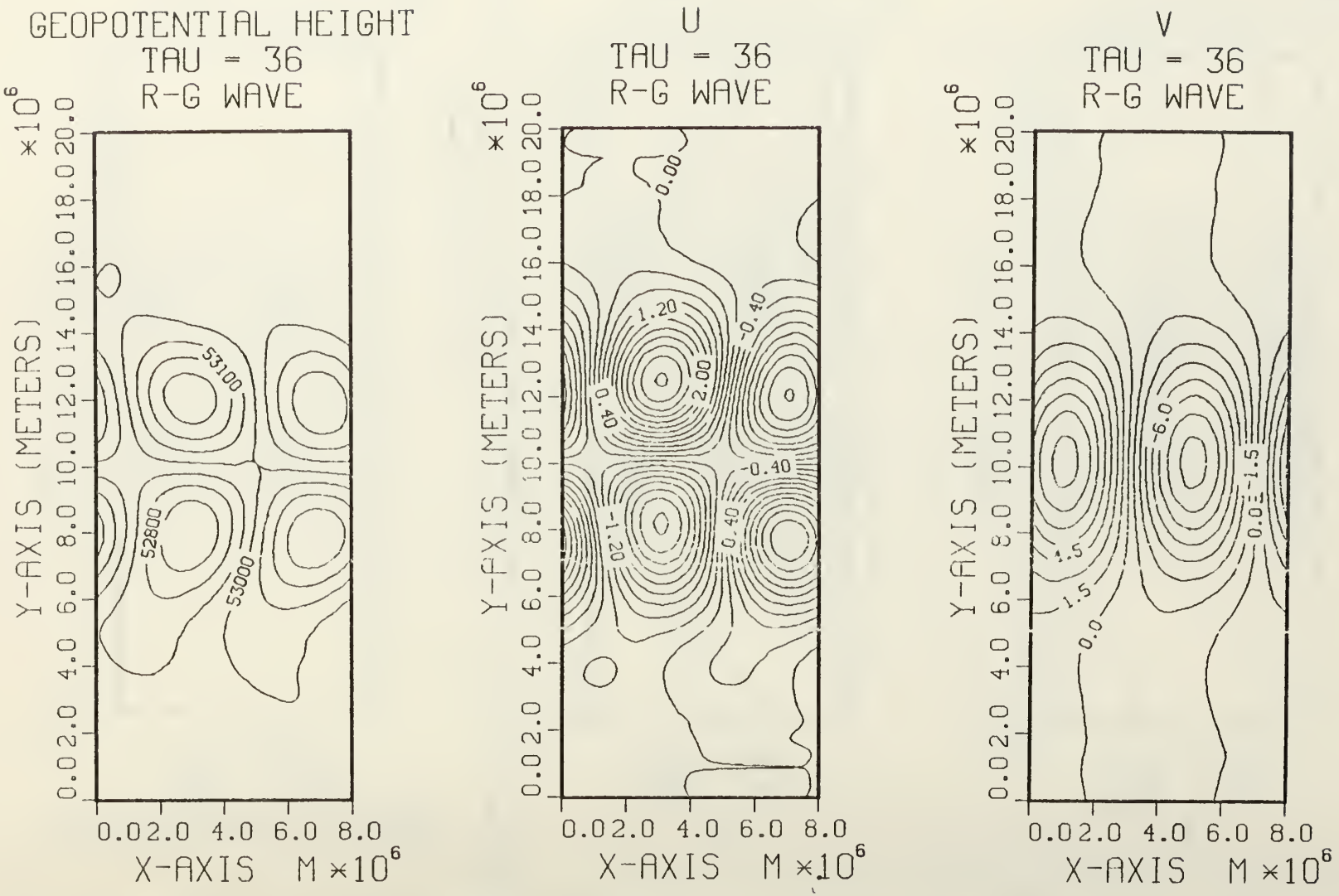

Figure 25. 25a, 25b, 25c, same as Figures 24a, 24b, 24c except at hour 36

III. Discussion

A dynamical method of initialization has been used to study the problem of initializing inertia-gravity motions. This problem is not of such high priority at the present time in NWP, but will become more so in the future because interest is increasing in the prediction of a) meso-scale phenomena in midlatitudes and b) tropical motions of all types. In the latter case Kelvin and Rossby-gravity type waves at or near the equator cause problems in all methods of conventional balance type initialization and objective analyses schemes. Here it is demonstrated that for Kelvin and Rossby-gravity waves the dynamic initialization does a very adequate job of recapturing the mass field near the equator. For operational needs however, several further considerations would have to be investigated. In these experiments perfect wind observations were always assumed. To relax this assumption leads into the area of problems related to objective analyses. In this connection Anthes (1976) has proposed in his work on hurricane simulation a method - called "nudging" - useful for both objective analysis and initialization. In essence this method adds another coefficient to the last term in equation (4) so it would be of the form, $C(\alpha,x,y,t)\ K_\alpha\ (\alpha_*^{n+1} - \alpha^o)$ where the C's would vary from grid point to grid point and would reflect a "confidence" factor in the observations. This idea could be incorporated into the procedure used in this paper. Also it must be acknowledged that this procedure might best be applied in conjunction - not opposition to - the best method of obtaining balanced winds and mass fields. Certainly this would be of great aid in those areas between observed data points.

Before final comments a brief point regarding the use of the Euler backward scheme. If a standard Von Neumann stability analysis is carried out for the Euler backward scheme, the results shows $|\lambda|^2 = \sqrt{1-\sigma^2 + \sigma^4} \leq 1$ where

$$\sigma = C \frac{\Delta t}{\Delta X} \sin \frac{2\pi \Delta X}{L} .$$

In the situation of the later runs, the approximate speed of the pure gravity wave, Cg, is about 230 m/sec with Δt = 360 sec and $\Delta X \equiv$ 444 kilometers. Therefore $Cg(\Delta t/\Delta X)$ is only about .2 near the equator. Even where $\sin(2\pi\Delta X/L) = 1$ (for $L = 4\ \Delta X$), $\sqrt{1 - \sigma^2 + \sigma^4} \cong .98$ so there is not much damping in these runs for these waves. For smaller values of C or longer waves up to $L = 18\ \Delta X$ the damping is even less significant. This is mentioned to emphasize that runs could be easily designed to take greater advantage of the damping than was done for the cases run here.

Finally, it may be of interest to investigate use of this initialization procedure using other types of models such as spectral or finite element models. Though there is no physical reason to believe it would not work, these types of models often make use of a semi-implicit scheme which slows down the inertia gravity waves considerably. How this might affect the process may be of interest. Use of split-explicit schemes however should be no formal problem. Here the external gravity mode is still explicitly predicted. In the case of the spectral formulation restoration coefficients might be formed directly on the basis of scale considerations relative to the Rossby radius of deformation in both directions. All these areas of further research seem promising.

References

Anthes, R. A., 1976: Data Assimilation and Initialization of Hurricane Prediction Models. Journal of Atmospheric Science, 31, pp 702-719.

Arakawa, A., 1971: Design of the UCLA General Circulation Model, Appendix A. Proposal to the NSF for Research on General Circulation, UCLA, Dept. of Meteorology, Aug. 1971, 123 pp. available on request.

Arakawa, A. and Lamb V., 1977: Computational Design of the Basic Dynamical Processes of the UCLA General Circulation Model, Methods in Computational Physics, Vol 17, Academic Press, 174-265, 337 pp.

Cahn, A., 1945: An Investigation of the Free Oscillations of a Simple Current System, Journal of Meteorology, Vol 2, No 2, June 1945, pp 113-119.

Haltiner, G. J. and Williams, R. T., 1980: Numerical Prediction and Dynamic Meteorology, 2nd Edition, John Wiley and Sons.

Hinkleman, K., 1951: Der Mechanismes des Meteorolgischen Larmes, Tellus, Vol 3, pp 285-296.

Machenhauer, B., 1977: On the Dynamics of Gravity Oscillations in a Shallow Water Model, with Application to Normal Mode Initialization, Contributions to Atmospheric Physics, Vol 50, pp 253-271.

Matsuno, T., 1966: Quasi-geostrophic Motions in the Equatorial Area, Journal of the Meteorological Society of Japan, Vol 44, pp 25-43.

Miyakoda, K., and Moyer, R. W., 1968: A Method of Initialization for Dynamical Weather Prediction, Tellus, Vol 20, No. 1, Jan 1968, pp 115-128.

Nitta, T., and Hovermale, J., 1969: A Technique of Objective Analysis and Initialization for the Primitive Forecast Equations, Monthly Weather Review, Vol 97, No. 9, Sept 1969, pp 652-658.

Winninghoff, F. J., 1968: On the Adjustment Toward a Geostrophic Balance in a Simple PE Model with Application to the Problems of Initialization and Objective Analysis, PhD Thesis, Dept. of Meteorology, UCLA, Dec 1968, 161 pp.

Winninghoff, F. J., 1973a: Note on a Simple Restorative-Iterative Procedure for Initialization of a Global Forecast Model, Monthly Weather Review, Vol 101, Jan 1973, pp 79-84.

Winninghoff, F. J., 1973b: On Inclusion of Restorative Coefficients and Physical Forcing into an Iterative Technique for Initialization of a Global Numerical Prediction Model, Canadian Meteorological Research Reports, 21 Nov 1973, 22 pp.

Distribution List

		No. Copies
1.	Defense Technical Information Center Cameron Station Alexandria, Virginia 22314	2
2.	Library, Code 0142 Naval Postgraduate School Monterey, California 93940	2
3.	Dr. R. T. Williams, Code 63Wu Department of Meteorology Naval Postgraduate School Monterey, California 93940	5
4.	Director Naval Oceanography and Meteorology National Space Technology Laboratories Bay St. Louis, Mississippi 39520	1
5.	Officer in Charge Naval Environmental Prediction Research Facility Monterey, California 93940	1
6.	Commanding Officer Fleet Numerical Oceanography Center Monterey, California 93940	1
7.	Naval Oceanographic Office Library, Code 3330 Washington, D.C. 20373	1
8.	AFCRL Research Library ATTN: Nancy Davis/Stop 29 L. G. Hanscom Field Bedford, Massachusetts 01730	1
9.	Commander, Air Weather Service Military Airlift Command United States Air Force Scott Air Force Base, Illinois 62226	1
10.	Dr. A. Arakawa Department of Meteorology University of California Los Angeles, California 90024	1

11. Atmospheric Sciences Library — 1
National Oceanic and Atmospheric Administration
Silver Spring, Maryland 20910

12. Dr. John Brown — 1
National Meteorological Center/NOAA
World Weather Building
Washington, D.C. 20233

13. Dr. C.-P. Chang, Code 63Cp — 1
Department of Meteorology
Naval Postgraduate School
Monterey, California 93940

14. Dr. R. L. Elsberry, Code 63Es — 1
Department of Meteorology
Naval Postgraduate School
Monterey, California 93940

15. Dr. R. L. Haney, Code 63Hy — 1
Department of Meteorology
Naval Postgraduate School
Monterey, California 93940

16. CDR D. Hinsman — 1
Naval Environmental Prediction Research Facility
Monterey, California 93940

17. Dr. B. J. Hoskins — 1
Department of Geophysics
University of Reading
Reading, United Kingdom

18. Dr. A. Kasahara — 1
National Center for Atmospheric Research
P.O. Box 3000
Boulder, Colorado 80303

19. Dr. M. G. Wurtele — 1
Department of Meteorology
University of California
Los Angeles, California 90024

20. Meteorology Reference Center, Code 63 — 1
Naval Postgraduate School
Monterey, California 93940

21. Dr. R. Madala — 1
Code 7750
Naval Research Laboratories
Washington, D.C. 20390

22. National Center for Atmospheric Research — 1
P.O. Box 1470
Boulder, Colorado 80302

23. Director, Naval Research Laboratory — 1
ATTN: Technical Services Information Center
Washington, D.C. 20390

24. Department of Oceanography, Code 68 — 1
Naval Postgraduate School
Monterey, California 93940

25. Office of Naval Research — 1
Department of the Navy
Washington, D.C. 20360

26. Prof. N. A. Phillips — 1
National Meteorological Center/NOAA
World Weather Building
Washington, D.C. 20233

27. Dr. K. Miyakoda — 1
Geophysical Fluid Dynamics Laboratory
Princeton University
Princeton, New Jersey 08540

28. Dr. T. Rosmond — 1
Naval Environmental Prediction Research Facility
Monterey, California 93940

29. Dr. D. Williamson — 1
National Center for Atmospheric Research
P.O. Box 3000
Boulder, Colorado 80303

30. Dr. Y. Sasaki — 1
Department of Meteorology
University of Oklahoma
Norman, Oklahoma 73069

31. Prof. A. L. Schoenstadt, Code 63Zh — 1
Naval Postgraduate School
Monterey, California 93940

32. Dr. M. J. P. Cullen — 2
Meteorological Office
Bracknell, Berks,
United Kingdom

33. Dr. R. L. Lee — 1
Atmospheric and Geophysical Science Division
University of California
P.O. Box 808
Livermore, California 94550

34. Prof. R. J. Renard, Code 63Rd — 1
Department of Meteorology
Naval Postgraduate School
Monterey, California 93940

35. Dr. C. H. Wash, Code 63Wx — 1
Department of Meteorology
Naval Postgraduate School
Monterey, California 93940

36. Dr. Andrew Staniforth — 1
Recherce en Prevision Numerique
West Isle Office Tower, 5 ieme etage
2121 route Trans-Canada
Dorval, Quebec H9P1J3, Canada

37. Dr. A. Weinstein — 1
Naval Environmental Prediction Research Facility
Monterey, California 93940

38. Dr. F. J. Winninghoff, Code 63Wn — 10
Department of Meteorology
Naval Postgraduate School
Monterey, California 93940

39. Dr. W. Blumen — 1
Campus Box 391
University of Colorado
Boulder, Colorado 80309

40. Dr. E. Barker — 1
Naval Environmental Prediction Research Facility
Monterey, California 93940

41. Mr. R. Hodur — 1
Naval Environmental Prediction Research Facility
Monterey, California 93940